Genomic landscape of tumor-host interactions with differential prognostic and predictive connotations

Jessica Roelands[1,2*], Wouter Hendrickx[1,3*#], Peter J.K. Kuppen[2], Raghvendra Mall[4], Gabriele Zoppoli[5,6], Mohamad Saad[4], Kyle Halliwill[7], Giuseppe Curigliano[8,9], Darawan Rinchai[1], Julie Decock[10], Lucia G Delogu[11], Tolga Turan[7], Josue Samayoa[7], Lotfi Chouchane[12], Ena Wang[13], Pascal Finetti[14], Francois Bertucci[14], Lance D Miller[15], Jerome Galon[16], Francesco M Marincola[17], Michele Ceccarelli[7#], Davide Bedognetti[1,3#]

1. Department of Immunology, Inflammation and Metabolism, Division of Translational Medicine, Research Branch, Sidra Medicine, Doha, Qatar
2. Department of Surgery, Leiden University Medical Center, Leiden, The Netherlands
3. College of Health and Life Sciences (CHLS), Hamad Bin Khalifa University (HBKU), Doha, Qatar.
4. Qatar Computing Research Institute, Hamad Bin Khalifa University, Doha, Qatar
5. IRCCS Ospedale Policlinico San Martino, Genova, Italy
6. Department of Internal Medicine, University of Genova, Genova, Italy
7. Computational Biology, Computational Oncology and Immunology (CIAO), AbbVie Biotherapeutics, Inc, Redwood City, California, United States of America
8. University of Milano, Department of Oncology and Hemato-Oncology
9. European Institute of Oncology, IRCCS, Milano, Italy
10. Cancer Research Center, Qatar Biomedical Research Institute (QBRI), Hamad Bin Khalifa University (HBKU), Qatar Foundation (QF), Doha, Qatar.
11. Istituto di Ricerca Pediatrica, Fondazione Città della Speranza, Padua, Italy
12. Laboratory of Genetic Medicine and Immunology, Weill Cornell Medicine-Qatar, Qatar
13. Allogene Therapeutics, South San Francisco, California
14. Department of Molecular Oncology, Institut Paoli-Calmettes, Centre de Recherche en Cancerologie de Marseille, UMR1068 Inserm, Marseille, France
15. Wake Forest Comprehensive Cancer Center, Winston-Salem, NC, USA.
16. INSERM, Laboratory of Integrative Cancer Immunology, Equipe Labellisée Ligue Contre le Cancer, Sorbonne Université, Sorbonne Paris Cité, Université Paris Descartes, Université Paris Diderot; Centre de Recherche des Cordeliers, F-75006 Paris, France
17. Refuge Biotechnologies, Menlo Park, California, 94025

[#] Corresponding authors
Davide Bedognetti: dbdognetti@sidra.org
Wouter Hendrickx: whendrickx@sidra.org
Michele Ceccarelli: mceccarelli@abbvie.com

* Equal contribution

Abstract

An immune active cancer phenotype typified by a T helper 1 (Th-1) immune response has been associated with increased responsiveness to immunotherapy and favorable prognosis in some but not all cancer types. The reason of this differential prognostic connotation remains unknown. Through a multi-modal Pan-cancer analysis among 31 different histologies (9,282 patients), we demonstrated that the favorable prognostic connotation conferred by the presence of a Th-1 immune response was abolished in tumors displaying specific tumor-cell intrinsic attributes such as high TGF-ß signaling and low proliferation capacity. This observation was validated in the context of immune-checkpoint inhibition. WNT-ß catenin, barrier molecules, Notch, hedgehog, mismatch repair, telomerase activity, and AMPK signaling were the pathways most coherently associated with an immune silent phenotype together with mutations of driver genes including *IDH1/2, FOXA2, HDAC3, PSIP1, MAP3K1, KRAS, NRAS, EGFR, FGFR3, WNT5A*, and *IRF7*. Our findings could be used to prioritize hierarchically relevant targets for combination therapies and to refine stratification algorithms.

Keywords

- Pan-cancer
- Immunologic Constant of Rejection
- Prognosis
- Mutational load
- Neoantigen load
- Aneuploidy
- Tumor intrinsic pathway enrichment
- Cancer Immunotherapy

67 **Introduction**

68 Evidence of the effects of anti-tumoral immunity on cancer progression has accumulated
69 over the last decades. The identification of tumor immune escape mechanisms, most
70 importantly the characterization of immune checkpoints, led to major advances in
71 immunotherapy. Immune checkpoint inhibitors have dramatically improved clinical outcome
72 for a subset of patients across multiple cancer types. Despite this progress, the majority of
73 patients (60-80%) still fail to respond (Emens et al., 2017; Gong et al., 2018). Understanding
74 the relationship between tumor cell and the immune system is critical to develop more effective
75 therapeutic strategies.

76 A pre-existing intratumoral anti-tumor immune response has been associated with
77 favorable outcome and responsiveness to immunotherapy (Galon et al., 2013). However,
78 multiple studies have reported differences in the association between measures of
79 intratumoral immune activity and survival across different cancer types (Charoentong et al.,
80 2017; Danaher et al., 2018; Tamborero et al., 2018; Thorsson et al., 2018; Varn et al., 2017).
81 In breast cancer, a positive association between survival and density of tumor infiltrating
82 lymphocytes, as estimated by transcriptomic data, was restricted to tumors displaying a high
83 mutational load or an aggressive/high proliferative phenotype (Miller et al., 2016; Nagalla et
84 al., 2013; Thomas et al., 2018). Proposed transcriptome-based immunological classifications
85 range from a measure of cytolytic activity by mean expression of *GZMA* and *PRF1* genes
86 (Rooney et al., 2015), to reflections of immune cell infiltration by cell-specific transcriptional
87 profiles (Bindea et al., 2013; Nagalla et al., 2013), or gene signatures reflecting molecular
88 components of an active antitumor immune response, including Major Histocompatibility
89 Complex (MHC), co-stimulatory or immunomodulatory molecules (Ayers et al., 2017;
90 Charoentong et al., 2017; Wang et al., 2008). Reported prognostic and predictive signatures
91 typically show overlapping genes or genes involved in conserved immunologic processes
92 (Bedognetti et al., 2016, 2013; Galon et al., 2013; Wang et al., 2013b, 2013a). We termed
93 these mechanisms as the Immunologic Constant of Rejection (ICR) (Galon et al., 2013; Wang
94 et al., 2008). The ICR signature incorporates IFN-stimulated genes driven by transcription
95 factors *IRF1* and *STAT1*, *CCR5* and *CXCR3* ligands, immune effector molecules, and counter-
96 activated immune regulatory genes (Hendrickx et al., 2017; Turan et al., 2018; Wang et al.,
97 2013b, 2008). Overall, the high expression of ICR typifies "hot"/immune active tumors
98 characterized by the presence of a T helper 1 (Th-1)/cytotoxic immune response, as described
99 in detail elsewhere (Bertucci et al., 2018; Galon et al., 2013; Hendrickx et al., 2017; Turan et
100 al., 2018).

101 Previously, we observed a significantly prolonged survival of patients with tumors
102 displaying a coordinated expression of ICR genes in breast cancer (Bertucci et al., 2018;
103 Hendrickx et al., 2017). Moreover, we identified genetic determinants of different immune

phenotypes (Hendrickx et al., 2017). In particular, we reported that transcriptional dysregulation of the MAPK pathways sustained by genetic alterations (i.e., MAP3K1 and MAP2K4 mutations) are enriched in immune silent tumors (Hendrickx et al., 2017). We also observed that the ICR signature refines and improves the prognostic value of conventional prognostic signatures adopted in breast cancer (Bertucci et al., 2018). Here, we propose a systematic analysis of the entire TCGA cohort encompassing 31 different histologies. Using a pan-cancer approach, we identified novel relationships between tumor genetic programs and immune orientation. After having demonstrated differential associations between ICR classification and overall survival across cancer types, we systemically analyzed in which (molecular) contexts ICR has prognostic value and in which ones it does not. Combination of immune orientation with tumor intrinsic attributes that interact with its prognostic significance could refine tumor immunologic classifications. This approach was validated in the context of immune-checkpoint inhibition allowing better predictive precision.

117 **Results**

118 *Prognostic impact of ICR classification is different between cancer types*

119 RNA-seq data of samples from a total of 9,282 patients across 31 distinct solid cancer
120 types were obtained from TCGA. To classify cancer samples based on their immune
121 orientation, we performed unsupervised consensus clustering for each cancer type separately
122 based on the expression of the ICR immune gene signature. This signature consists of 20
123 genes that reflect activation of Th1-signaling (*IFNG*, *TXB21*, *CD8B*, *CD8A*, *IL12B*, *STAT1,* and
124 *IRF1*), CXCR3/CCR5 chemokine ligands (*CXCL9*, *CXCL10,* and *CCL5*), cytotoxic effector
125 molecules (*GNLY*, *PRF1*, *GZMA*, *GZMB,* and *GZMH*) and compensatory immune regulators
126 (*CD274/PD-L1, PDCD1, CTLA4, FOXP3*, and *IDO1*) (**Figure 1A**) (Bedognetti et al., 2016;
127 Galon et al., 2013; Hendrickx et al., 2017; Turan et al., 2018). Expression of these genes
128 showed a positive correlation with each other across all cancer types (**Supplementary Figure**
129 **1**). The ICR signature highly correlates with other immune signatures that aim to reflect a
130 highly active immune tumor microenvironment, including the Tumor Inflammation Signatures
131 (TIS) (r = 0.97)(Danaher et al., 2018) (**Supplementary Figure 2**). As a representative
132 example, consensus clustering and cluster assignment of skin cutaneous melanoma (SKCM)
133 is shown in **Figure 1A**. Analogous figures for each of the 31 cancer types are available as
134 cancer datasheets at figshare.com.

135 As shown in **Figure 1B**, the mean expression of ICR genes, or ICR score, varies
136 between cancer types, reflecting general differences in tumor immunogenicity between
137 cancers. While brain tumors (brain lower grade glioma's (LGG) and glioblastoma multiforme
138 (GBM)) typically display low immunological signals (McGranahan et al., 2017), skin cutaneous
139 melanoma (SKCM) and head and neck squamous cell carcinoma (HNSC) display high levels
140 of immune activation (Economopoulou et al., 2016; Passarelli et al., 2017; Thorsson et al.,
141 2018). In addition, the distribution of ICR scores among patients and the difference between
142 the highest and lowest ICR scores varies between cancers. Accordingly, the proportions of
143 patients assigned to specific ICR clusters are dependent on the cancer type. Even more
144 clinically relevant, the relation of the different immune phenotypes to survival is dissimilar
145 among cancer types (**Figure 1C-D**). While the ICR High phenotype (hot) shows a significant
146 survival benefit compared with the ICR Low phenotype (cold) for various cancer types (BRCA,
147 SKCM, UCEC, SARC), the ICR High cluster is associated with significantly reduced overall
148 survival in other cancer types (UVM, LGG, PAAD, KIRC) (**Figure 1C**). Similar results were
149 obtained when Cox regression analysis was performed on ICR score as a continuous variable
150 (**Supplementary Table 1**). To explore biological differences between cancer types in which a
151 highly active immune phenotype is mostly associated with favorable survival and cancer types
152 in which this phenotype is mostly associated with decreased survival, we categorized cancer
153 types in ICR-*enabled* (BRCA, SKCM, UCEC, SARC, LIHC, HNSC, STAD, BLCA) and ICR-

154 *disabled* (UVM, LGG, PAAD, KIRC) groups, respectively (**Figure 1C**). All other cancer types
155 in which ICR did not show an association or trend were categorized as ICR-*neutral*. Of
156 important note, this classification was used for explorative purposes, a role of the immune
157 mediated tumor rejection cannot be precluded in ICR-neutral cancer types.

158 First, we explored whether the ICR scores and their distributions were different among
159 these defined groups of cancer types. Mean ICR score is low for most ICR-disabled (ranging
160 from 3.97 to 8.34) compared to ICR-enabled cancer types (ranging from 7.26 to 8.36)
161 (**Supplementary Figure 3A**). This observation is most noticeable for ICR-disabled cancer
162 types LGG and UVM. Moreover, the difference (delta) between ICR scores in ICR High
163 compared to ICR Low groups is higher in ICR-enabled cancer types (range: 2.98-4.97)
164 compared to ICR-neutral (range: 1.48-4.49) and ICR-disabled cancer types (range: 2.29-3.35)
165 (**Supplementary Figure 3B**). These factors could underlie, at least partially, the observed
166 divergent associations with survival.

167 To define whether tumor pathologic stage might interact with the association between
168 ICR and overall survival (OS), we fitted a Cox proportional hazards model for each group of
169 ICR-enabled, ICR-neutral and ICR-disabled cancer types (**Table 1**). Overall, including ICR
170 High and ICR Low samples from all cancer types, ICR has significant prognostic value
171 independent of AJCC pathologic stage. For ICR-enabled cancer types, the ICR High group
172 also remains significantly associated with improved survival after adjusting for tumor
173 pathologic stage. For ICR-disabled cancer types, ICR High was associated with worse survival
174 in univariate analysis (HR <1). However, in multivariate models this negative prognostic value
175 of ICR was lost (HR=1.054; 95% CI= 0.7702- 1.443). Kaplan-Meier plots stratified by
176 pathologic stage showed that within individual pathologic stages, ICR was not associated with
177 OS for ICR-disabled cancers (**Supplementary Figure 4.1**). In fact, in the ICR-disabled tumors
178 (but not in the ICR-enabled ones), ICR was significantly higher (p = 10 e-7) in advanced vs
179 early stages (**Supplementary Figure 4.2**). Similarly, a progressive enrichment of ICR high
180 samples was observed with more advanced stages in the ICR-disables tumors UVM and
181 KIRC, and, in, LGG with more advanced grades.

182 For ICR-neutral cancer types, while ICR was not associated with survival in univariate
183 analysis, multivariate analysis indeed identified a positive prognostic value of the ICR
184 classification, though less robust than observed for ICR-enabled cancer types.

FIG1

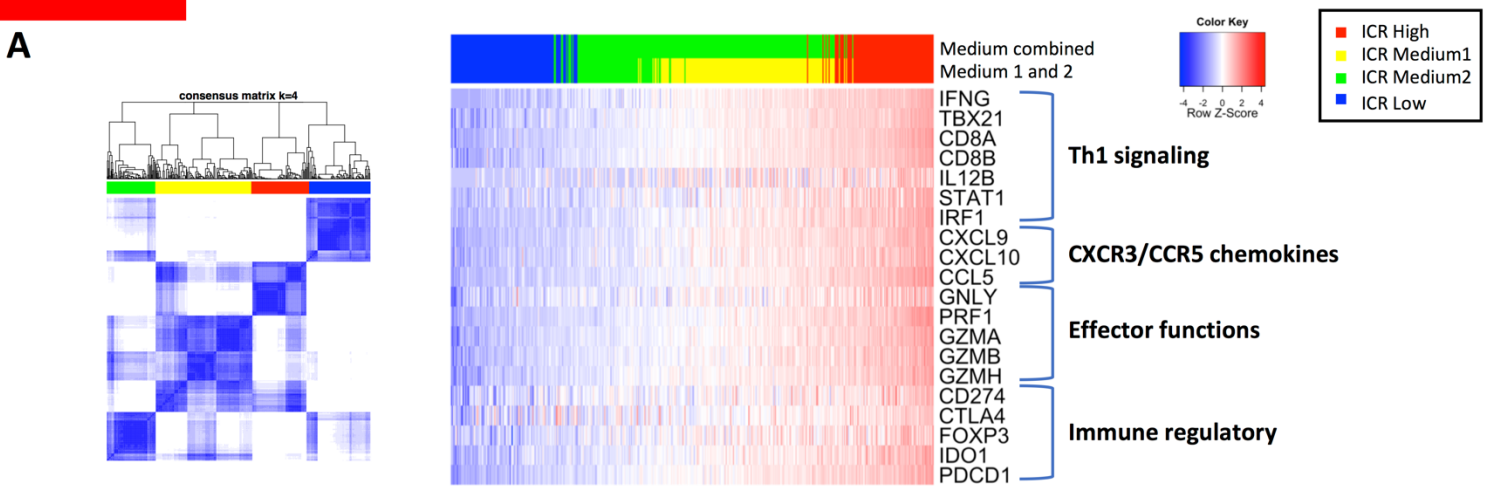

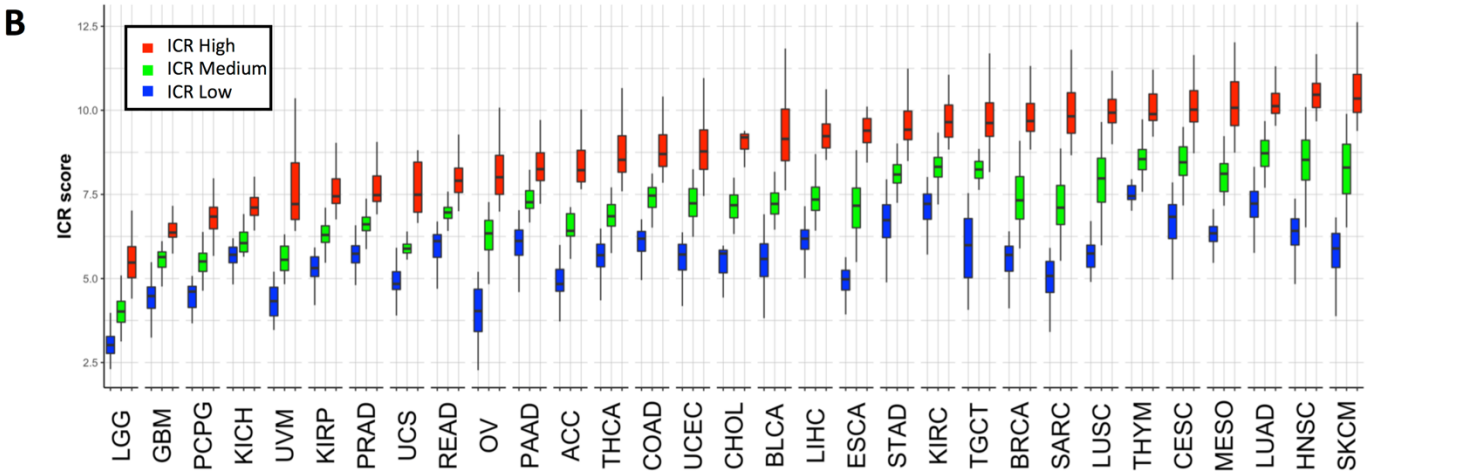

C

	Cancer	N	N ICR High	N ICR Low	p–value	HR
ICR disabled	UVM	80	28	30	0.000221	0.0567
	LGG	513	101	189	3.29e–05	0.353
	PAAD	156	23	82	0.0379	0.542
	KIRC	515	134	139	0.0273	0.621
	PRAD	493	94	218	0.638	0.651
	KIRP	285	87	60	0.477	0.745
	MESO	87	11	25	0.7	0.856
	GBM	153	34	62	0.675	0.903
	ESCA	182	28	22	0.873	0.929
	UCS	57	13	27	0.946	0.969
	LUAD	510	70	234	0.978	0.994
	COAD	276	80	81	0.603	1.18
	READ	89	46	20	0.799	1.2
	LUSC	486	76	47	0.503	1.22
	OV	302	125	43	0.356	1.24
ICR enabled	BLCA	404	148	146	0.0573	1.4
	STAD	401	112	181	0.0994	1.41
	HNSC	514	95	118	0.0949	1.43
	KICH	65	38	15	0.575	1.51
	CESC	301	99	68	0.249	1.53
	ACC	78	7	46	0.504	1.64
	CHOL	36	7	12	0.451	1.67
	LIHC	368	59	92	0.0483	1.77
	SARC	254	48	49	0.0643	1.95
	UCEC	173	59	45	0.0946	2.25
	SKCM	469	96	114	1.2e–05	2.89
	BRCA	1082	152	266	0.00163	3.01
	THCA	500	128	159	0.136	3.25

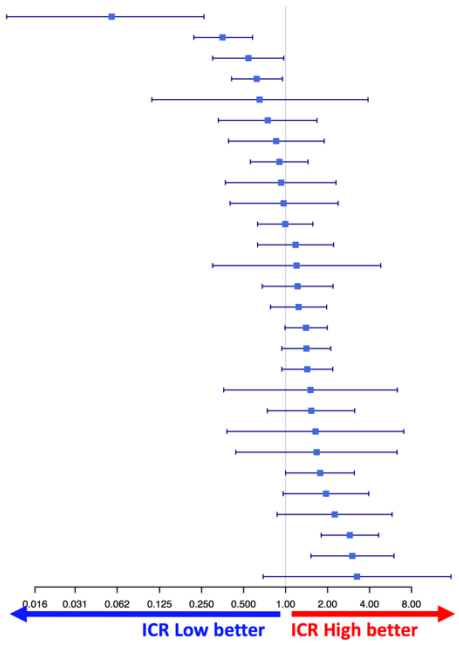

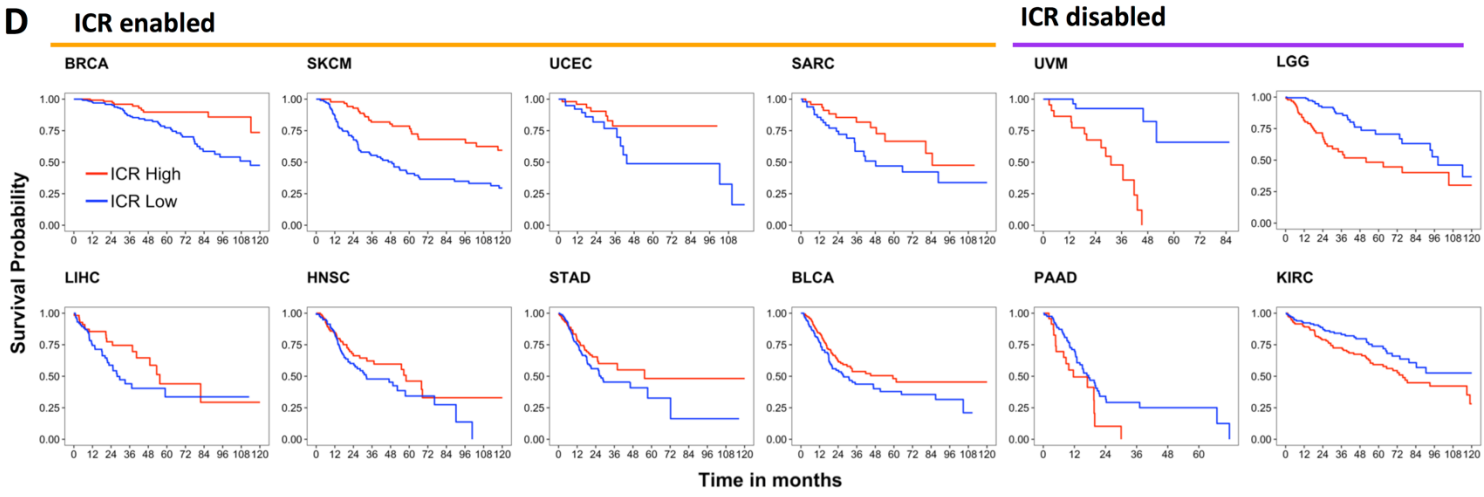

Table 1. Cox proportional hazards regression for association with overall survival in ICR-enabled and ICR-disabled tumors: ICR High and ICR Low samples included (ICR Medium samples excluded).

	Univariable		Multivariable	
Variables	**HR (95% CI)**	***p***	**HR (95% CI)**	***p***
ICR overall (n = 4735)				
~ ICR cluster (ICR Low vs. High)	1.203 (1.081-1.339)	0.00073 ***	1.343 (1.180- 1.528)	7.85e-06 ***
~ Pathologic stage (Stage I, II, III, IV)	1.72 (1.615-1.832)	<2e-16 ***	1.716 (1.611- 1.827)	<2e-16 ***
Samples from ICR-enabled cancer types (n = 1742)				
~ ICR cluster (ICR Low vs. High)	1.631(1.374-1.937)	2.26e-8 ***	1.488 (1.233- 1.795)	3.35e-05 ***
~ Pathologic stage (Stage I, II, III, IV)	1.817 (1.644-2.008)	<2e-16 ***	1.798 (1.628- 1.987)	<2e-16 ***
Samples from ICR-disabled cancer types (n = 721)				
~ ICR cluster (ICR Low vs. High)	0.6194 (0.4801-0.7992)	0.000229 ***	1.054 (0.7702- 1.443)	0.742
~ Pathologic stage (Stage I, II, III, IV)	1.55 (1.351-1.778)	4.22e-10 ***	1.560 (1.3520- 1.801)	1.19e-9 ***
Samples from ICR neutral cancer types (n = 2272)				
~ ICR cluster (ICR Low vs. High)	1.160 (0.983-1.369)	0.0789	1.336 (1.065- 1.676)	0.0122 *
~ Pathologic stage (Stage I, II, III, IV)	1.665 (1.5-1.848)	<2e-16 ***	1.640 (1.477- 1.821)	<2e-16 ***

Signif. codes: *** <0.001; ** <0.01; * <0.05

ICR cluster entered as categorical (factor) variable (factor levels: “ICR High”, “ICR Low”)
Pathologic stage as semi-continuous variable (Stage I = 1; Stage II = 2; Stage III = 3; Stage IV = 4)
LGG and GBM were not included, as tumor stage is not available (not applicable) for these cancer types.

198 *ICR reflects anti-tumor immune activity and is inversely correlated with tumor-related*
199 *pathways associated with immune escape*

200 To further explore differences between cancer types, we aimed to compare the density
201 of leukocyte subpopulations between ICR High and Low samples across cancers. Gene
202 expression signatures specific to 24 cell types (Bindea et al., 2013) were used to deconvolute
203 the abundance of immune cells in tumor samples by performing single sample gene set
204 enrichment analysis (ssGSEA) (Barbie et al., 2009). Cell-specific enrichment scores (ES) for
205 each patient demonstrated a clear enrichment of transcripts specific to T- and B cells in ICR
206 High patients (**Figure 2A**). More specifically, ICR High samples showed increased expression
207 of transcripts associated with cytotoxic T cells, T-regulatory (T-reg) cells, Th1 cells, NK
208 CD56dim cells, activated dendritic cells (aDC) and macrophages, compared with ICR Medium
209 and ICR Low samples. This observation is consistent across cancer types, in both ICR-
210 enabled and ICR-disabled cancers. So, in addition to the immune functional molecular
211 orientation, the ICR gene signature is a good reflection of anti-tumor immune cell infiltration
212 (Lu et al., 2017). To quantitatively compare immune cell enrichment between individual cancer
213 types, the mean ES was calculated for each cancer type (**Supplementary Figure 5**). Overall,
214 no single consistent difference in terms of immune cell enrichment can be observed that can
215 discriminate ICR-enabled from ICR-disabled cancer types. LGG and UVM show an overall
216 low immune infiltration, consistent with our reported low ICR scores.

217 We then proceeded to examine which tumor intrinsic attributes correlate with immune
218 phenotype as reflected by ICR gene expression. We performed ssGSEA to identify enrichment
219 of transcripts of common tumor-related pathways (Hendrickx et al., 2017; Lu et al., 2017;
220 Salerno et al., 2016). Not surprisingly, immune-related pathways including TNFR1 Signaling
221 and immunogenic cell death showed a strong positive correlation with expression of ICR
222 genes (**Figure 2B**). This implies that our immune signature captures the anti-tumoral
223 immunological processes well across a wide range of cancer types. Interestingly, few
224 pathways were identified that inversely correlated with ICR gene expression, potentially
225 representing mechanisms by which immune silent tumors develop their phenotype. These
226 pathways include WNT-β catenin (Corrales et al., 2017; Spranger and Gajewski, 2015), barrier
227 genes (Salerno et al., 2016), AMPK signaling (Dandapani and Hardie, 2013), mismatch repair,
228 telomerase extension by telomerase, Notch, and Hedgehog, signaling pathways. Of special
229 note, genes that we previously found to be upregulated in MAP3K1/MAP2K4-mutated vs wild-
230 type (wt) breast cancer which perfectly segregated ICR High versus Low samples in the BRCA
231 TCGA cohort (MAPK-up genes) (Hendrickx et al., 2017), were also inversely correlated with
232 ICR in a significant proportion of cancers (i.e, ACC, THYM, GBM, LGG and TGCT).

FIG2

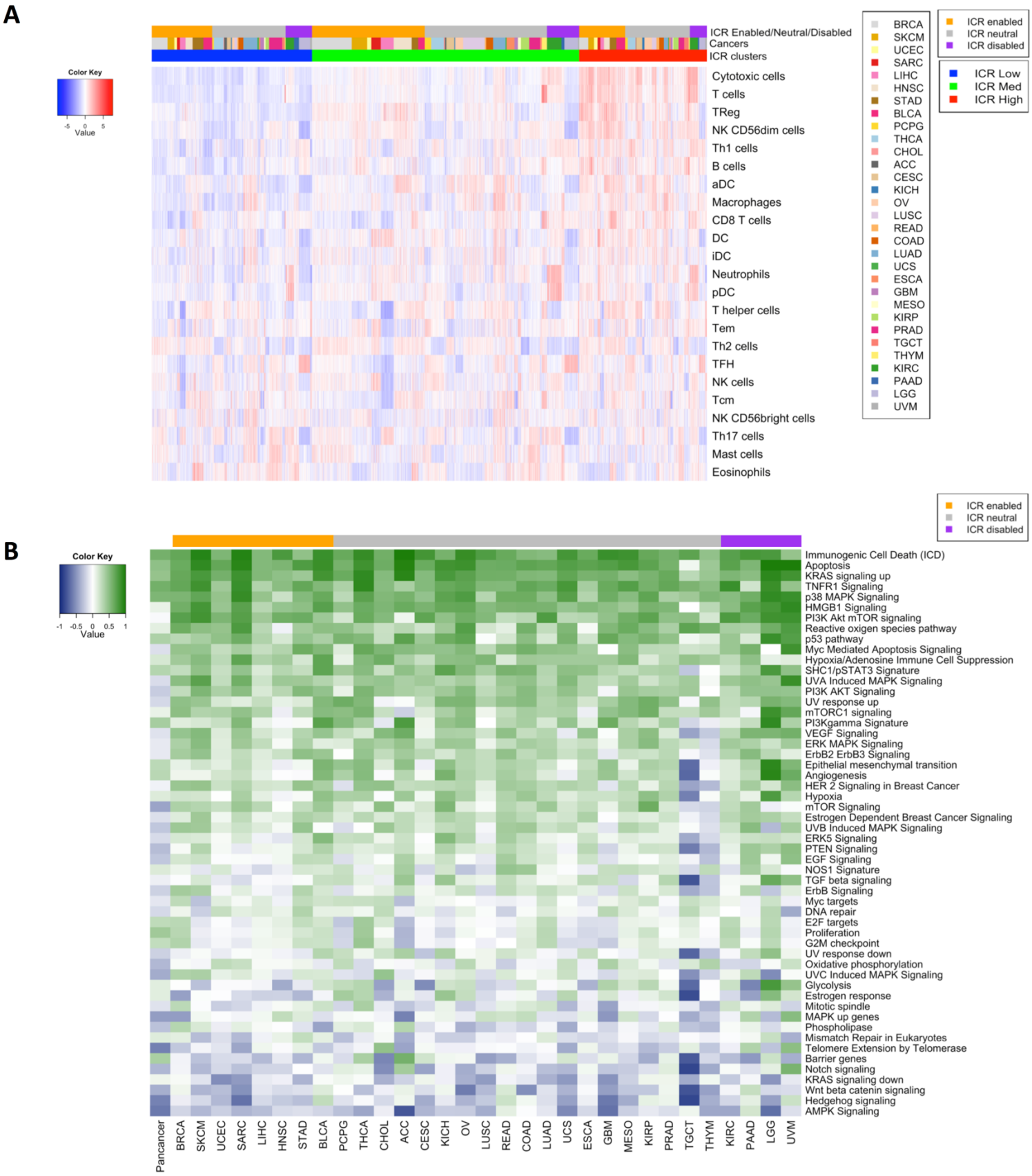
A
Color Key
-5 0 5
Value
ICR Enabled/Neutral/Disabled
Cancers
ICR clusters
Cytotoxic cells
T cells
TReg
NK CD56dim cells
Th1 cells
B cells
aDC
Macrophages
CD8 T cells
DC
iDC
Neutrophils
pDC
T helper cells
Tem
Th2 cells
TFH
NK cells
Tcm
NK CD56bright cells
Th17 cells
Mast cells
Eosinophils
BRCA
SKCM
UCEC
SARC
LIHC
HNSC
STAD
BLCA
PCPG
THCA
CHOL
ACC
CESC
KICH
OV
LUSC
READ
COAD
LUAD
UCS
ESCA
GBM
MESO
KIRP
PRAD
TGCT
THYM
KIRC
PAAD
LGG
UVM
ICR enabled
ICR neutral
ICR disabled
ICR Low
ICR Med
ICR High
B
Color Key
-1 -0.5 0 0.5 1
Value
ICR enabled
ICR neutral
ICR disabled
Immunogenic Cell Death (ICD)
Apoptosis
KRAS signaling up
TNFR1 Signaling
p38 MAPK Signaling
HMGB1 Signaling
PI3K Akt mTOR signaling
Reactive oxigen species pathway
p53 pathway
Myc Mediated Apoptosis Signaling
Hypoxia/Adenosine Immune Cell Suppression
SHC1/pSTAT3 Signature
UVA Induced MAPK Signaling
PI3K AKT Signaling
UV response up
mTORC1 signaling
PI3Kgamma Signature
VEGF Signaling
ERK MAPK Signaling
ErbB2 ErbB3 Signaling
Epithelial mesenchymal transition
Angiogenesis
HER 2 Signaling in Breast Cancer
Hypoxia
mTOR Signaling
Estrogen Dependent Breast Cancer Signaling
UVB Induced MAPK Signaling
ERK5 Signaling
PTEN Signaling
EGF Signaling
NOS1 Signature
TGF beta signaling
ErbB Signaling
Myc targets
DNA repair
E2F targets
Proliferation
G2M checkpoint
UV response down
Oxidative phosphorylation
UVC Induced MAPK Signaling
Glycolysis
Estrogen response
Mitotic spindle
MAPK up genes
Phospholipase
Mismatch Repair in Eukaryotes
Telomere Extension by Telomerase
Barrier genes
Notch signaling
KRAS signaling down
Wnt beta catenin signaling
Hedgehog signaling
AMPK Signaling
Pancancer
BRCA
SKCM
UCEC
SARC
LIHC
HNSC
STAD
BLCA
PCPG
THCA
CHOL
ACC
CESC
KICH
OV
LUSC
READ
COAD
LUAD
UCS
ESCA
GBM
MESO
KIRP
PRAD
TGCT
THYM
KIRC
PAAD
LGG
UVM

234 *Characterization of tumor mutational load and aneuploidy in relation to ICR immune*
235 *phenotypes*

236 Next, we aimed to identify genomic attributes related to the ICR immune phenotypes.
237 As previously observed (Thorsson et al., 2018), mean neoantigen count of each cancer type
238 strongly correlated with mean mutation rate (**Supplementary Figure 6A-B**). While mean non-
239 silent mutation rate was significantly higher in ICR High tumors for some cancer types, no
240 clear association was observed in most of them. Results for predicted neoantigen load were
241 similar (**Figure 3A-B** and **Supplementary Figure 6C-D**). Overall, mean non-silent mutation
242 rate and mean neoantigen load were higher in ICR-enabled cancers compared with ICR-
243 disabled cancers. However, these differences cannot fully explain the divergent association
244 of ICR with survival, as values for ICR-enabled cancers SARC and BRCA are in the same
245 range as ICR-disabled cancers LGG, PAAD and KIRC.

246 Similarly, we studied the association between genomic instabilities, or aneuploidy, and
247 ICR. Specifically, we compared the individual tumor aneuploidy scores and the ICR score
248 across cohorts. Aneuploidy score was calculated as in Taylor *et al* (Taylor et al., 2018). As
249 has been reported previously, we found a broad negative association between aneuploidy and
250 raw or tumor purity adjusted ICR score (Davoli et al., 2017) (**Figure 3C**). Interestingly, this
251 negative association was most strongly supported in ICR-enabled cancers, with 6 cancers out
252 of 8 showing a significant negative association between aneuploidy score and purity adjusted
253 ICR ($P < 0.01$). In ICR-neutral cancers, a small fraction of cancer types showed a negative
254 association (4 of 18, with an additional 4 showing a non-significant but suggestive negative
255 association). Three cohorts (GBM, KICH and PRAD) showed a suggestive positive
256 association. Similarly, in the ICR-disabled cohorts only KIRC showed a significant negative
257 association, while LGG showed a strongly significant positive association (p-value $< 10^{-8}$).

FIG3

A

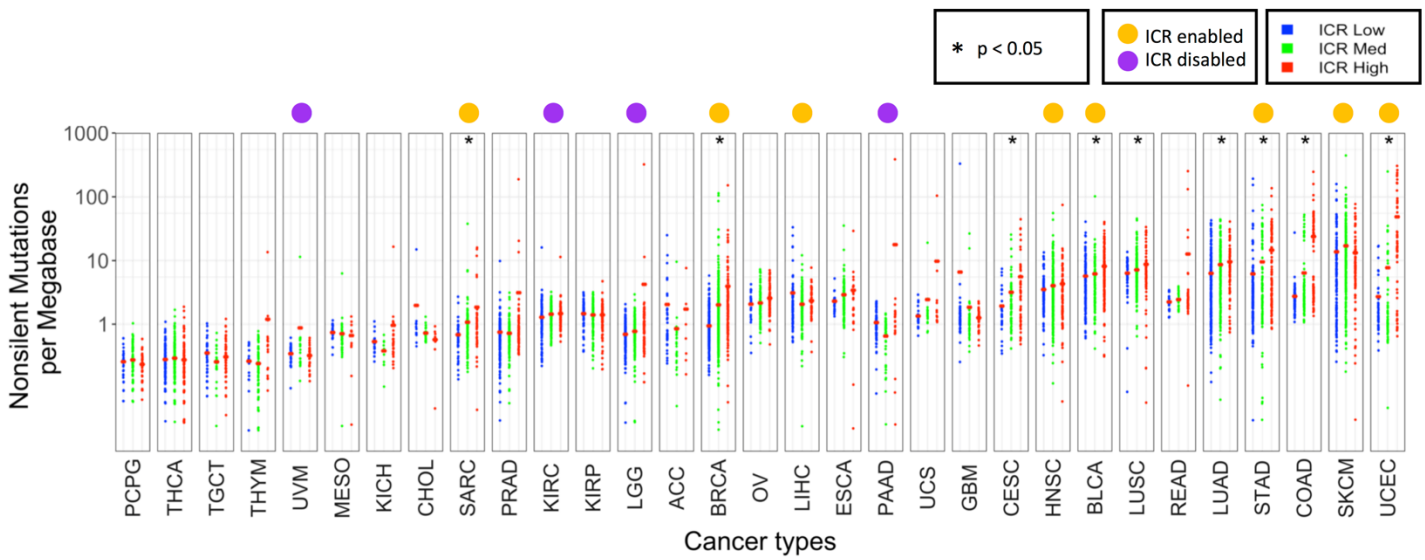
* p < 0.05
ICR enabled
ICR disabled
ICR Low
ICR Med
ICR High
Nonsilent Mutations per Megabase
1000
100
10
1
PCPG THCA TGCT THYM UVM MESO KICH CHOL SARC PRAD KIRC KIRP LGG ACC BRCA OV LIHC ESCA PAAD UCS GBM CESC HNSC BLCA LUSC READ LUAD STAD COAD SKCM UCEC
Cancer types

B

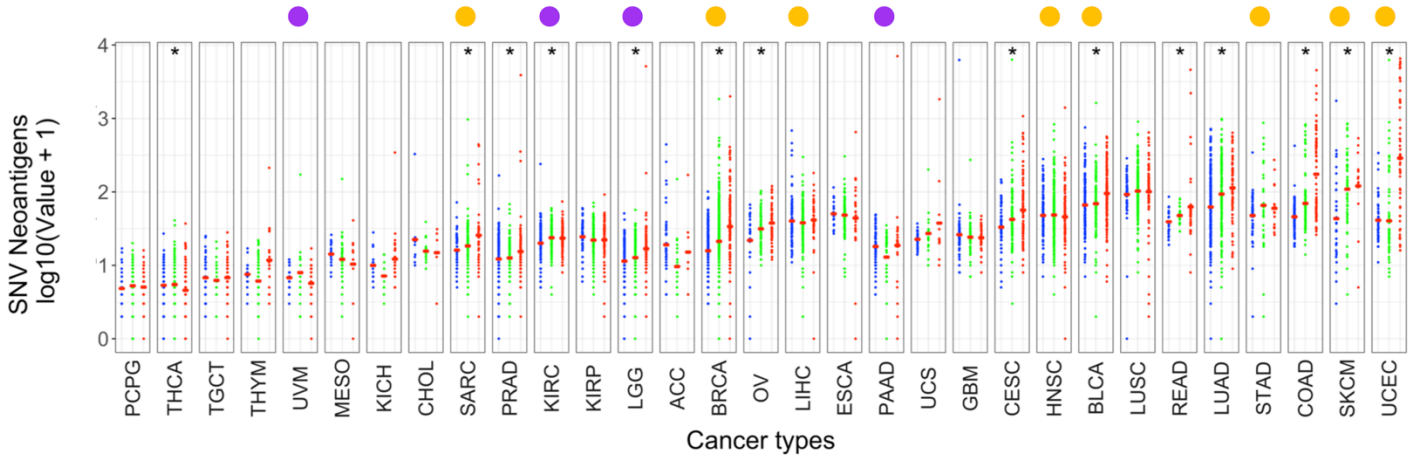
SNV Neoantigens log10(Value + 1)
4
3
2
1
0
PCPG THCA TGCT THYM UVM MESO KICH CHOL SARC PRAD KIRC KIRP LGG ACC BRCA OV LIHC ESCA PAAD UCS GBM CESC HNSC BLCA LUSC READ LUAD STAD COAD SKCM UCEC
Cancer types

C

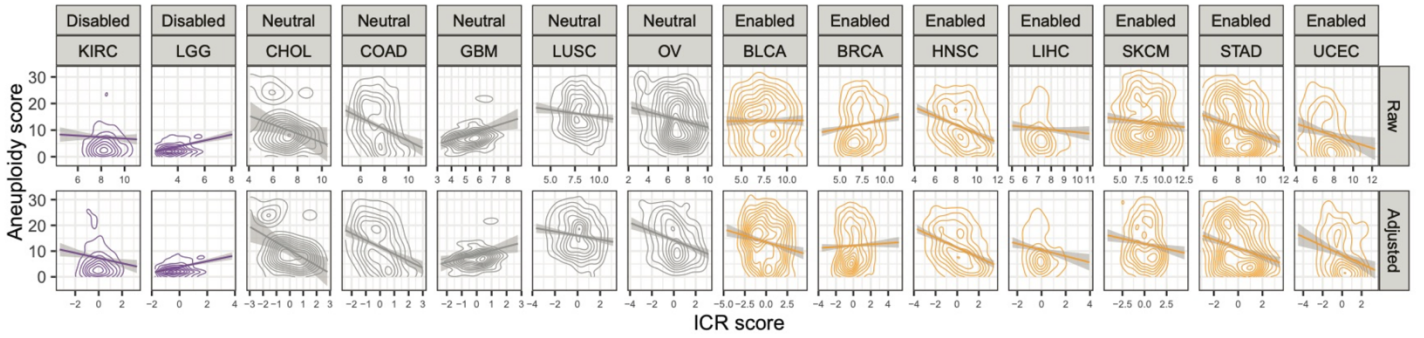
Disabled KIRC
Disabled LGG
Neutral CHOL
Neutral COAD
Neutral GBM
Neutral LUSC
Neutral OV
Enabled BLCA
Enabled BRCA
Enabled HNSC
Enabled LIHC
Enabled SKCM
Enabled STAD
Enabled UCEC
Raw
Adjusted
Aneuploidy score
ICR score

259 *Specific mutations associate with ICR immune phenotypes*

260 To define the association of specific oncogenic mutations with ICR immune
261 phenotypes, we first selected a set of 470 frequently mutated genes in cancer (Iorio et al.,
262 2016), then trained an elastic net (Zou and Hastie, 2005) model to predict the ICR score as
263 function of mutations in each sample and using the tumor-type as covariate. The positive non-
264 zero coefficients of the trained model were used to identify genes whose mutation are
265 associated with an increase of the ICR and negative non-zero coefficients identify the genes
266 whose mutations are associated to a decrease of the ICR score (**Figure 4A**). The use of
267 tumor-type as covariate tends to limit the effect of the enrichment of mutations in specific
268 cancer-types and their correlation with ICR score. The coefficients of the tumor-type were all
269 different from zero, with the exception of BLCA, BRCA, CHOL, COAD, READ and SARC and
270 retained in the final model. We evaluated the accuracy of the model in a ten-fold cross-
271 validation computing the correlation between the model prediction and the true ICR scores
272 and obtaining a Spearman correlation of 0.669 ± *0.012* (p-value < 10^{-400}). Genes associated
273 with a decrease of ICR score include: *FOXA2*, *NSD1*, *PSIP1*, *HDAC3*, *ZNF814*, *FRG1*,
274 *SOX17*, *CARM1*, *GATA3*, *FKBP5*, *FGFR3*, *MAT2A*, *PPP2R5A*, *MECOM*, *SMAD2*, *MED17*,
275 *WNT5A*, *KRAS*, *ADAM10*, *PRKAR1A*, *DIS3*, *PRRX1*, *MFNG*, *TNPO1*, *SPOP*, *KDM6A*, *EGFR*,
276 *IRF7*, *NRAS*, *SUZ12*, *RPSAP58*, and *SF3B1.*

277 Interestingly MAP3K1 mutations, whose effect on ICR Low has been described in
278 breast cancer (Hendrickx et al., 2017), were also associated to ICR Low tumors pan-cancer.
279 The top genes of which mutations positively correlate with ICR reflect immune-evasion
280 mechanisms that follow immunologic pressure such as mutations of antigen-presenting
281 machinery transcripts previously described (i.e., *B2M, HLA-A, HLA-B*, and *CASP8*)(Rooney
282 et al., 2015).

283 To better compare the association between specific mutations and ICR groups within
284 individual cancer types, we calculated, for each of the identified genes, the mean ICR score
285 in the mutated group divided by the mean ICR score in the wild type (WT) within each
286 individual cancer type. For most cancer types, the genes with a positive coefficient consistently
287 showed a higher ICR score in mutated samples, supporting their association with an ICR High
288 phenotype (**Figure 4B**). On the other hand, genes with a negative coefficient (genes
289 associated with an ICR Low phenotype) as identified at the pan-cancer level, do show some
290 clear deviations between cancer types. While for most cancer types, ICR score is indeed lower
291 in the mutated group, results for cancer types COAD, UCEC and STAD show the reverse
292 (**Figure 4B**). Interestingly, a common characteristic of these three cancer types is frequent
293 hypermutation as a consequence of microsatellite instability (MSI) (Cortes-Ciriano et al.,
294 2017). This hypermutator phenotype could be responsible for the observed increased ICR
295 score in the mutated group, as the genes with negative coefficient could be mutated in the

296 context of hypermutation. We indeed observed an increased ICR score in the MSI-high group
297 compared to MSI-low and microsatellite stable (MSS) groups in COAD and STAD datasets
298 for which sufficient data on MSI status were available (Cortes-Ciriano et al., 2017)
299 (**Supplementary Figure 7A-B**).
300 Mutated genes were frequently part of multiple pathways, suggesting impact on
301 various tumor biological systems (**Supplementary Figure 8**).

FIG4

A

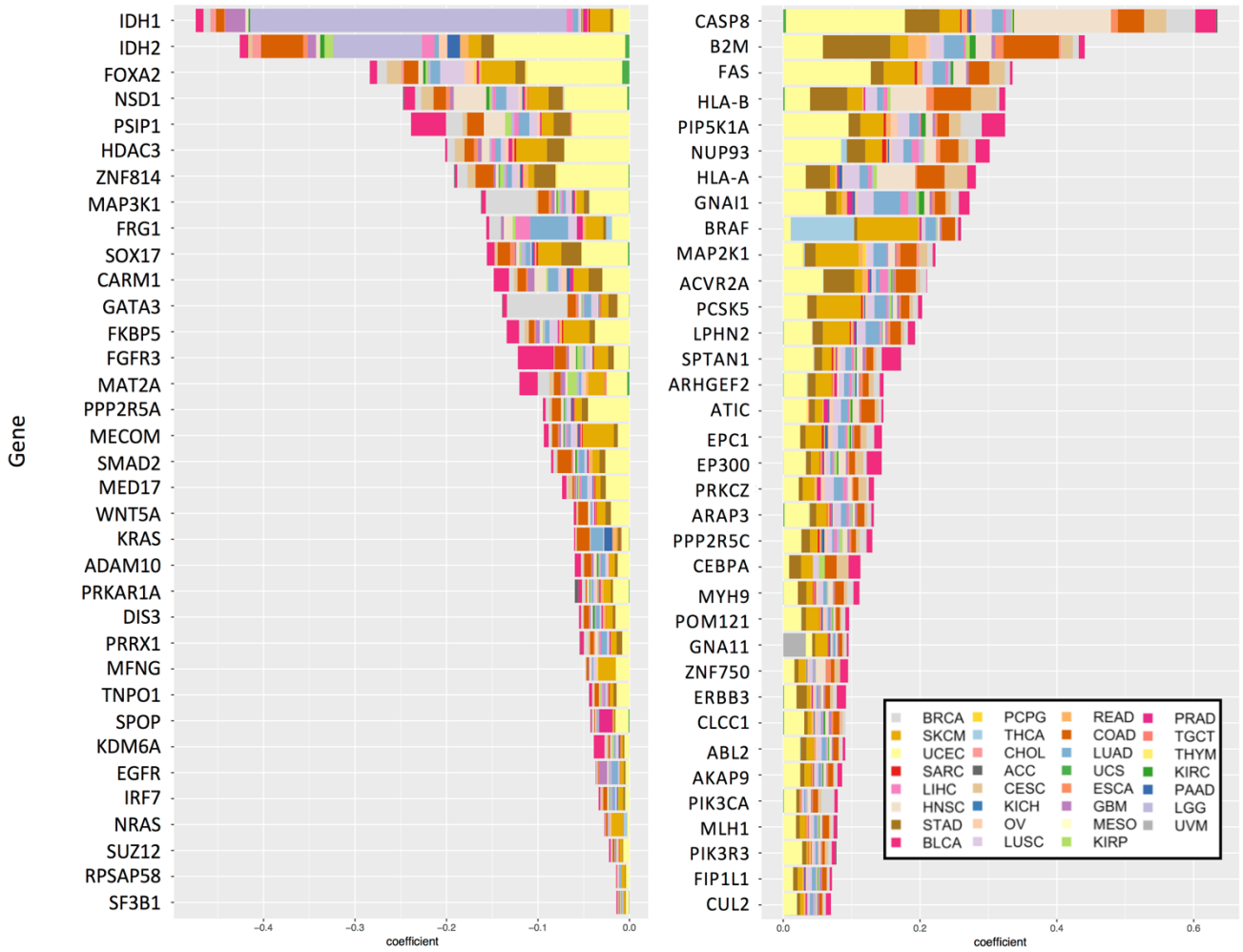
Gene
IDH1
IDH2
FOXA2
NSD1
PSIP1
HDAC3
ZNF814
MAP3K1
FRG1
SOX17
CARM1
GATA3
FKBP5
FGFR3
MAT2A
PPP2R5A
MECOM
SMAD2
MED17
WNT5A
KRAS
ADAM10
PRKAR1A
DIS3
PRRX1
MFNG
TNPO1
SPOP
KDM6A
EGFR
IRF7
NRAS
SUZ12
RPSAP58
SF3B1
−0.4
−0.3
−0.2
−0.1
0.0
coefficient
CASP8
B2M
FAS
HLA-B
PIP5K1A
NUP93
HLA-A
GNAI1
BRAF
MAP2K1
ACVR2A
PCSK5
LPHN2
SPTAN1
ARHGEF2
ATIC
EPC1
EP300
PRKCZ
ARAP3
PPP2R5C
CEBPA
MYH9
POM121
GNA11
ZNF750
ERBB3
CLCC1
ABL2
AKAP9
PIK3CA
MLH1
PIK3R3
FIP1L1
CUL2
0.0
0.2
0.4
0.6
coefficient
BRCA
SKCM
UCEC
SARC
LIHC
HNSC
STAD
BLCA
PCPG
THCA
CHOL
ACC
CESC
KICH
OV
LUSC
READ
COAD
LUAD
UCS
ESCA
GBM
MESO
KIRP
PRAD
TGCT
THYM
KIRC
PAAD
LGG
UVM

B

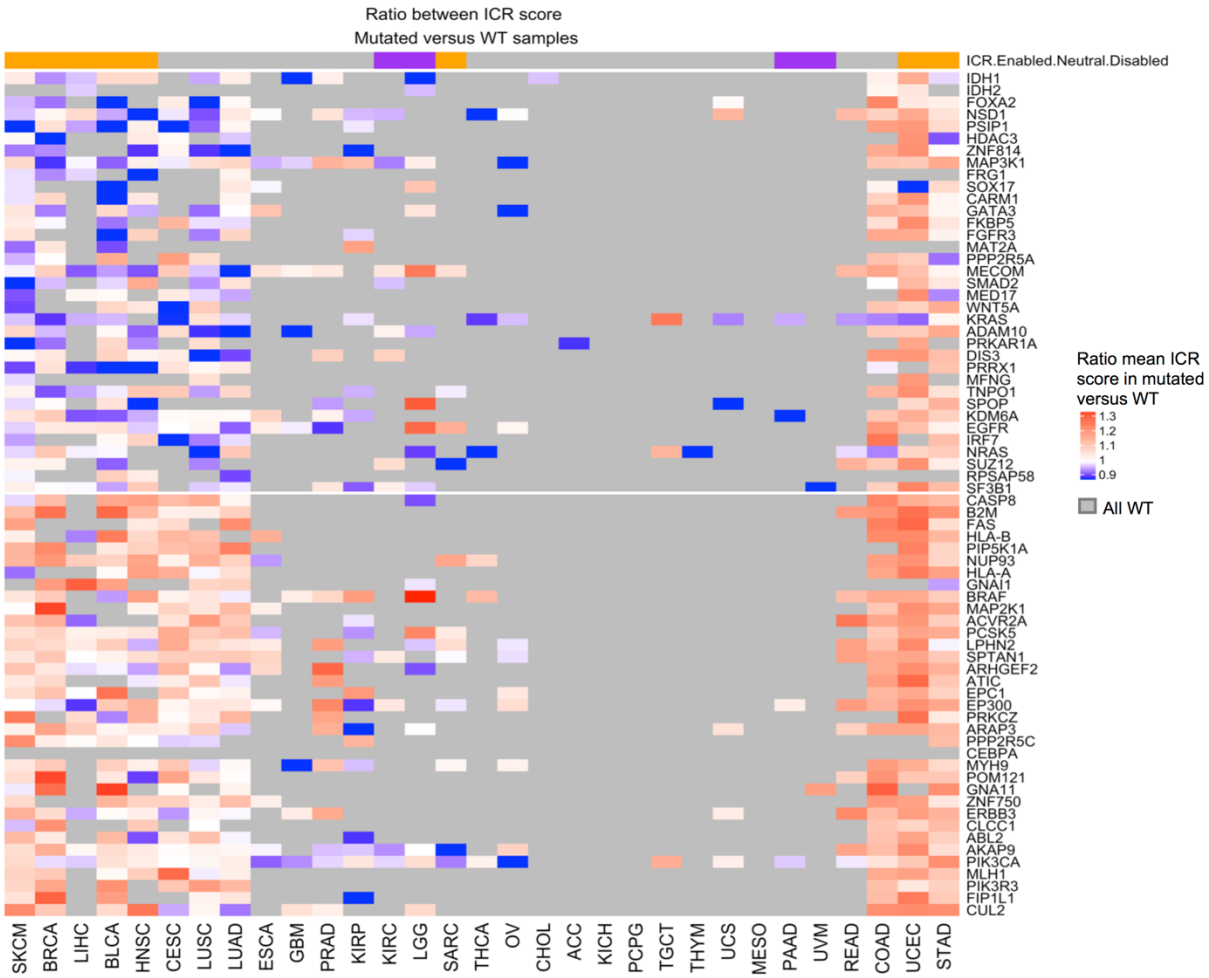
Ratio between ICR score
Mutated versus WT samples
ICR.Enabled.Neutral.Disabled
IDH1
IDH2
FOXA2
NSD1
PSIP1
HDAC3
ZNF814
MAP3K1
FRG1
SOX17
CARM1
GATA3
FKBP5
FGFR3
MAT2A
PPP2R5A
MECOM
SMAD2
MED17
WNT5A
KRAS
ADAM10
PRKAR1A
DIS3
PRRX1
MFNG
TNPO1
SPOP
KDM6A
EGFR
IRF7
NRAS
SUZ12
RPSAP58
SF3B1
CASP8
B2M
FAS
HLA-B
PIP5K1A
NUP93
HLA-A
GNAI1
BRAF
MAP2K1
ACVR2A
PCSK5
LPHN2
SPTAN1
ARHGEF2
ATIC
EPC1
EP300
PRKCZ
ARAP3
PPP2R5C
CEBPA
MYH9
POM121
GNA11
ZNF750
ERBB3
CLCC1
ABL2
AKAP9
PIK3CA
MLH1
PIK3R3
FIP1L1
CUL2
SKCM
BRCA
LIHC
BLCA
HNSC
CESC
LUSC
LUAD
ESCA
GBM
PRAD
KIRP
KIRC
LGG
SARC
THCA
OV
CHOL
ACC
KICH
PCPG
TGCT
THYM
UCS
MESO
PAAD
UVM
READ
COAD
UCEC
STAD
Ratio mean ICR score in mutated versus WT
1.3
1.2
1.1
1
0.9
All WT

303 *Prognostic impact of ICR classification is dependent on the expression of cancer-related*
304 *pathways*
305 Although we observed interesting differences between ICR High and ICR Low immune
306 phenotypes across different cancer types, these do not explain the divergent association
307 between immune phenotype and survival as we observed in ICR-enabled versus ICR-disabled
308 cancer types (**Figure 1C-D**). As previously stated, an active immune phenotype has different
309 impacts on survival depending on molecular subtype (for e.g. breast cancer (Miller et al.,
310 2016)). To examine tumor intrinsic differences between ICR-enabled and ICR-disabled cancer
311 types, we compared the enrichment of tumor intrinsic pathways between these two groups.
312 Differentially enriched pathways (t-test; FDR <0.05; **Supplementary Table 2**) between ICR-
313 enabled and disabled cancer types were selected and used for pan-cancer hierarchical
314 clustering. Interestingly, a wide variety of pathways were differentially enriched between both
315 groups. Whereas enrichment for pathways involved in proliferation were mostly upregulated
316 in ICR-enabled cancer types (proliferation metagene (Miller et al*.,* 2016), E2F targets, G2M
317 checkpoints and mismatch repair), a large number of tumor intrinsic pathways (n=43) were
318 enriched in ICR-disabled cancer types. Visualization of ES for these pathways across different
319 cancer types in a heatmap confirms these findings. Hierarchical clustering based on ES of
320 tumor intrinsic pathways differentially dysregulated by ICR-enabled and ICR-disabled cancer
321 types segregates specimens into two main clusters (**Figure 5A**). As anticipated, pan-cancer
322 survival analysis of all samples that formed a cluster along with samples of the ICR-disabled
323 cancer types, named the *ICR non-beneficial cluster*, revealed no survival benefit of a high ICR
324 expression. On the other hand, survival analysis of all samples in the other cluster, named the
325 *ICR beneficial cluster*, showed a clear survival benefit for ICR High samples (**Figure 5B**). Of
326 note, the prognostic significance of ICR was higher in this ICR beneficial cluster (HR = 1.82;
327 p-value = 4.13^{-9}; 95% CI = 1.49-2.23) compared to the prognostic significance of all samples
328 of ICR-enabled cancer types combined (HR = 1.63, p = 2.26^{-8}; 95% CI = 0.88-1.14),
329 suggesting that tumor intrinsic attributes beyond the tumor site of origin are important to
330 determine the relevance of cancer immune phenotypes. Interestingly, samples from ICR-
331 neutral cancers, in which no clear trend was observed between ICR and survival (**Figure 1C**),
332 and which were not used in calculation of differentially enriched pathways, were divided across
333 the *ICR beneficial* and *ICR non-beneficial clusters*. To evaluate whether the prognostic impact
334 of the ICR was relevant to a subset of samples from ICR-neutral cancer types, subgroup
335 analysis was performed for samples of ICR-neutral cancer types. Indeed, for all samples from
336 ICR-neutral cancer types that clustered to the *ICR non-beneficial cluster*, ICR was not
337 associated with survival. On the other hand, for samples of ICR-neutral cancer types which
338 clustered to the *ICR beneficial cluster*, ICR showed a significant positive association with

339 survival (**Figure 5C**), indicating that the ICR has prognostic relevance in this subgroup of
340 cancer patients as well.

FIG5

A

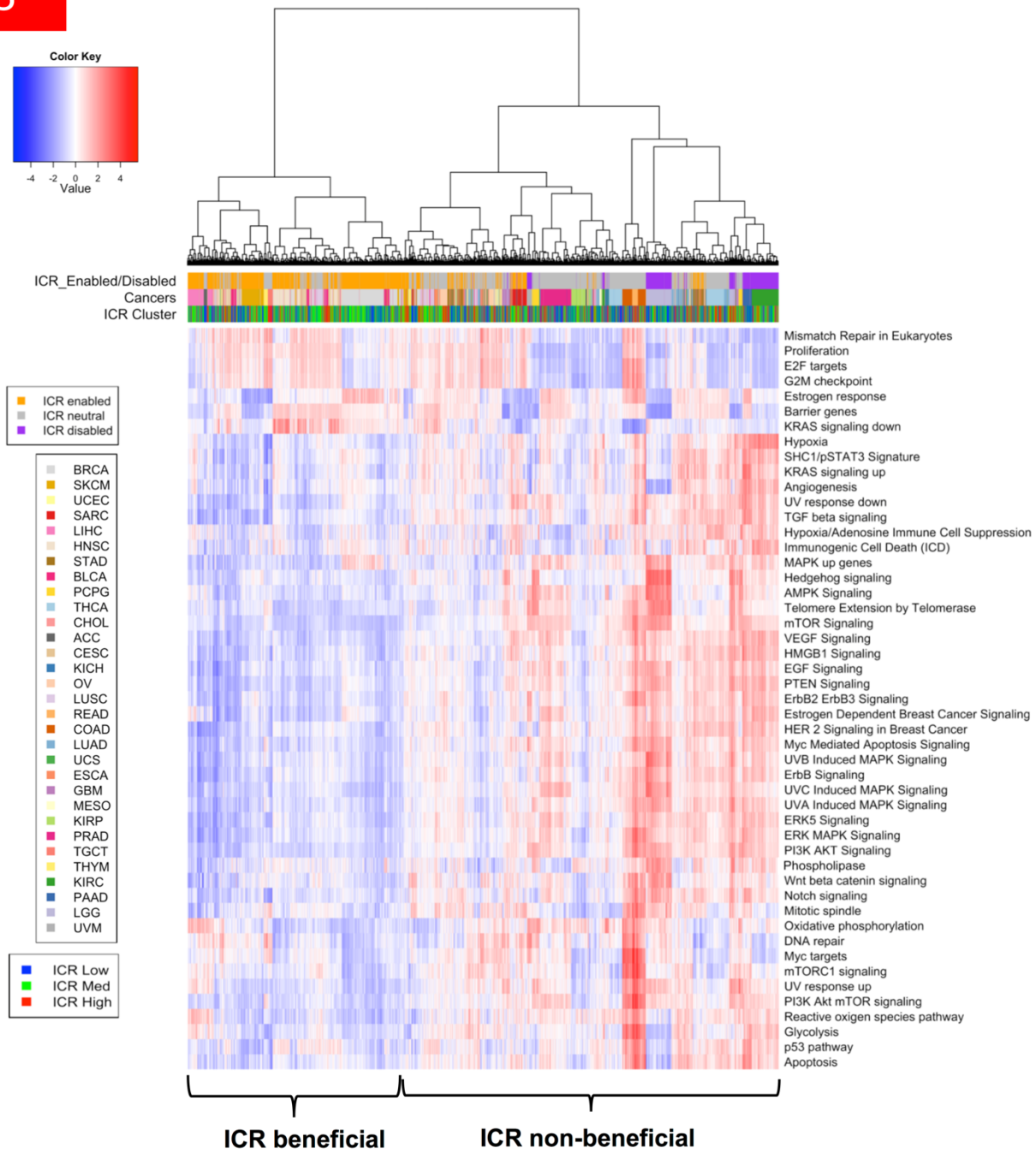
Color Key
-4 -2 0 2 4
Value
ICR_Enabled/Disabled
Cancers
ICR Cluster
ICR enabled
ICR neutral
ICR disabled
BRCA
SKCM
UCEC
SARC
LIHC
HNSC
STAD
BLCA
PCPG
THCA
CHOL
ACC
CESC
KICH
OV
LUSC
READ
COAD
LUAD
UCS
ESCA
GBM
MESO
KIRP
PRAD
TGCT
THYM
KIRC
PAAD
LGG
UVM
ICR Low
ICR Med
ICR High
Mismatch Repair in Eukaryotes
Proliferation
E2F targets
G2M checkpoint
Estrogen response
Barrier genes
KRAS signaling down
Hypoxia
SHC1/pSTAT3 Signature
KRAS signaling up
Angiogenesis
UV response down
TGF beta signaling
Hypoxia/Adenosine Immune Cell Suppression
Immunogenic Cell Death (ICD)
MAPK up genes
Hedgehog signaling
AMPK Signaling
Telomere Extension by Telomerase
mTOR Signaling
VEGF Signaling
HMGB1 Signaling
EGF Signaling
PTEN Signaling
ErbB2 ErbB3 Signaling
Estrogen Dependent Breast Cancer Signaling
HER 2 Signaling in Breast Cancer
Myc Mediated Apoptosis Signaling
UVB Induced MAPK Signaling
ErbB Signaling
UVC Induced MAPK Signaling
UVA Induced MAPK Signaling
ERK5 Signaling
ERK MAPK Signaling
PI3K AKT Signaling
Phospholipase
Wnt beta catenin signaling
Notch signaling
Mitotic spindle
Oxidative phosphorylation
DNA repair
Myc targets
mTORC1 signaling
UV response up
PI3K Akt mTOR signaling
Reactive oxigen species pathway
Glycolysis
p53 pathway
Apoptosis
ICR beneficial
ICR non-beneficial

B

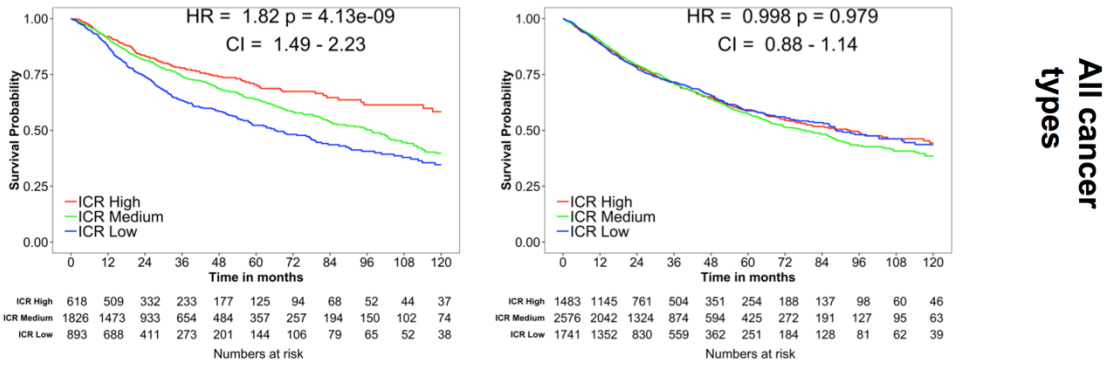
HR = 1.82 p = 4.13e-09
CI = 1.49 - 2.23
Survival Probability
ICR High
ICR Medium
ICR Low
Time in months
ICR High 618 509 332 233 177 125 94 68 52 44 37
ICR Medium 1826 1473 933 654 484 357 257 194 150 102 74
ICR Low 893 688 411 273 201 144 106 79 65 52 38
Numbers at risk
HR = 0.998 p = 0.979
CI = 0.88 - 1.14
ICR High 1483 1145 761 504 351 254 188 137 98 60 46
ICR Medium 2576 2042 1324 874 594 425 272 191 127 95 63
ICR Low 1741 1352 830 559 362 251 184 128 81 62 39
All cancer types

C

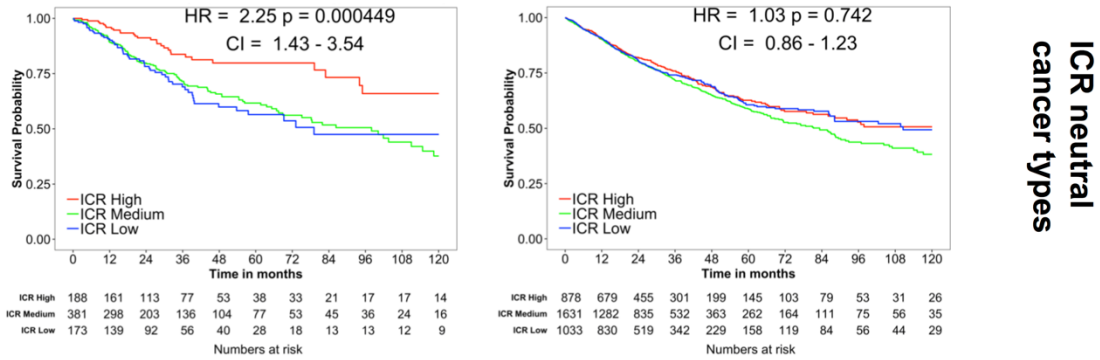
HR = 2.25 p = 0.000449
CI = 1.43 - 3.54
Survival Probability
ICR High
ICR Medium
ICR Low
Time in months
ICR High 188 161 113 77 53 38 33 21 17 17 14
ICR Medium 381 298 203 136 104 77 53 45 36 24 16
ICR Low 173 139 92 56 40 28 18 13 13 12 9
Numbers at risk
HR = 1.03 p = 0.742
CI = 0.86 - 1.23
ICR High 878 679 455 301 199 145 103 79 53 31 26
ICR Medium 1631 1282 835 532 363 262 164 111 75 56 35
ICR Low 1033 830 519 342 229 158 119 84 56 44 29
ICR neutral cancer types

343 To better clarify this concept, we selected two of the differentially expressed pathways
344 that were of special interest. Firstly, the “Proliferation” signature was used to classify all
345 samples independent of tumor origin in “Proliferation High” and “Proliferation Low” categories,
346 defined as an ES value >median or <median of all samples, respectively. This 52-gene cluster
347 described by Nagalla *et al* (Nagalla et al., 2013) has previously been associated with the
348 prognostic value of immune gene signatures in breast cancer (Miller et al., 2016). As
349 represented by a histogram, the proportion of samples with high proliferation signature
350 enrichment was larger in ICR-enabled cancer types compared with ICR-disabled cancers
351 (**Figure 6A**). This very basic binary classification was already capable of segregating samples
352 in a group in which ICR has a positive prognostic value from a group in which ICR is not
353 associated with survival (**Figure 6B**). As a second illustration, “TGF-ß signaling” was used to
354 classify samples based on this pathway using the same approach. For this oncogenic
355 pathway, ICR-enabled cancer types typically had a lower enrichment of this pathway
356 compared to ICR-disabled cancer types (**Figure 6C**). This classification could also divide
357 samples in a group in which ICR has a positive association with survival and a group in which
358 this association is absent (**Figure 6D**).
359 As proliferation positively correlates with tumor mutational load (Pearson’s correlation
360 coefficient = 0.49) (**Supplementary Figure 9**), we investigated whether tumor proliferation
361 independently contributes to the prognostic value of ICR. Therefore, we segregated pan-
362 cancer samples in four categories based on both mutation rate and proliferation
363 (**Supplementary Figure 10**). Interestingly, in the proliferation high group, ICR High was
364 associated with significantly improved survival independent of mutation rate. A similar
365 observation is made for the mutation rate high group, ICR High is associated with better
366 survival independent of proliferation. These finding suggest that mutation rate and enrichment
367 of proliferation-related transcripts provide additive information to define the prognostic value
368 of ICR. Furthermore, in a multivariate Cox proportional hazards model including ICR
369 classification, proliferation enrichment, TGF-ß signaling enrichment, and tumor mutation rate,
370 all parameters remain significant (**Supplementary Figure 11**). This implies that ICR,
371 proliferation rate, TGF-ß signaling and tumor mutation rate all have independent prognostic
372 value.
373 We then continued by verifying whether these tumor intrinsic attributes that interact
374 with the prognostic impact of ICR when evaluated pan-cancer, could also translate to
375 individual cancer types. For each individual cancer type, samples were divided by median ES
376 for each of the selected pathways. ICR HRs (ICR Low vs. ICR High) were compared between
377 each pathway-High and pathway-Low group for each cancer type (**Supplementary Figure**
378 **S12A-B**). Overall, we indeed observed an increased HR for samples with a high enrichment

379 of ICR enabling pathways for most cancer types. For samples with a high enrichment of ICR
380 disabling pathways, the HR was indeed lower (**Supplementary Figure S12C**).
381 These data confirm an association between the prognostic impact of ICR classification
382 and enrichment of oncogenic pathways in individual cancer types as well as pan-cancer. Of
383 note, these interactions between the prognostic significance of ICR and tumor intrinsic
384 pathways were mostly present in enabled and neutral cancer types. Within disabled cancer
385 types, with the exception of KIRC, similar associations were not found.

FIG6

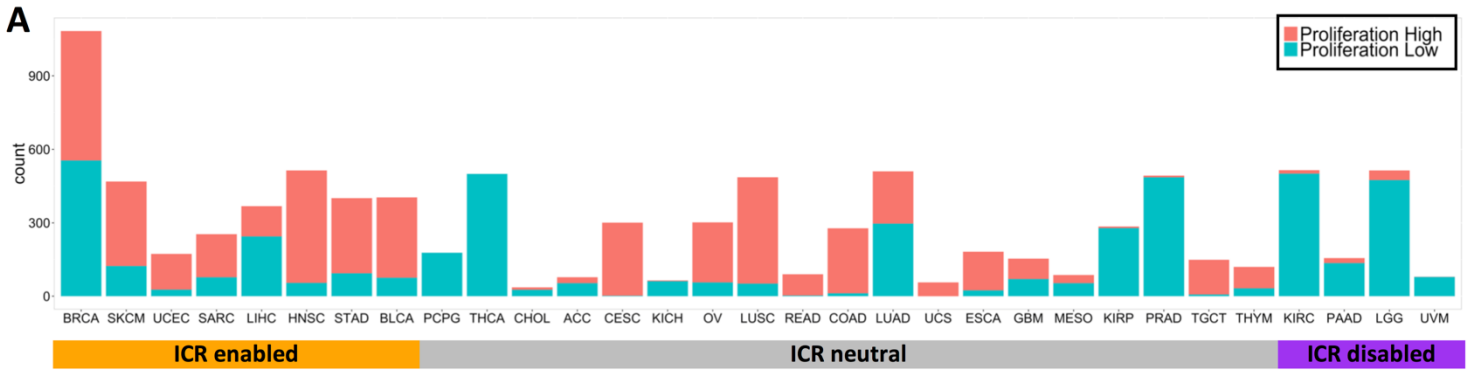
A
Proliferation High
Proliferation Low
count
900
600
300
0
BRCA SKCM UCEC SARC LIHC HNSC STAD BLCA PCPG THCA CHOL ACC CESC KICH OV LUSC READ COAD LUAD UCS ESCA GBM MESO KIRP PRAD TGCT THYM KIRC PAAD LGG UVM
ICR enabled
ICR neutral
ICR disabled

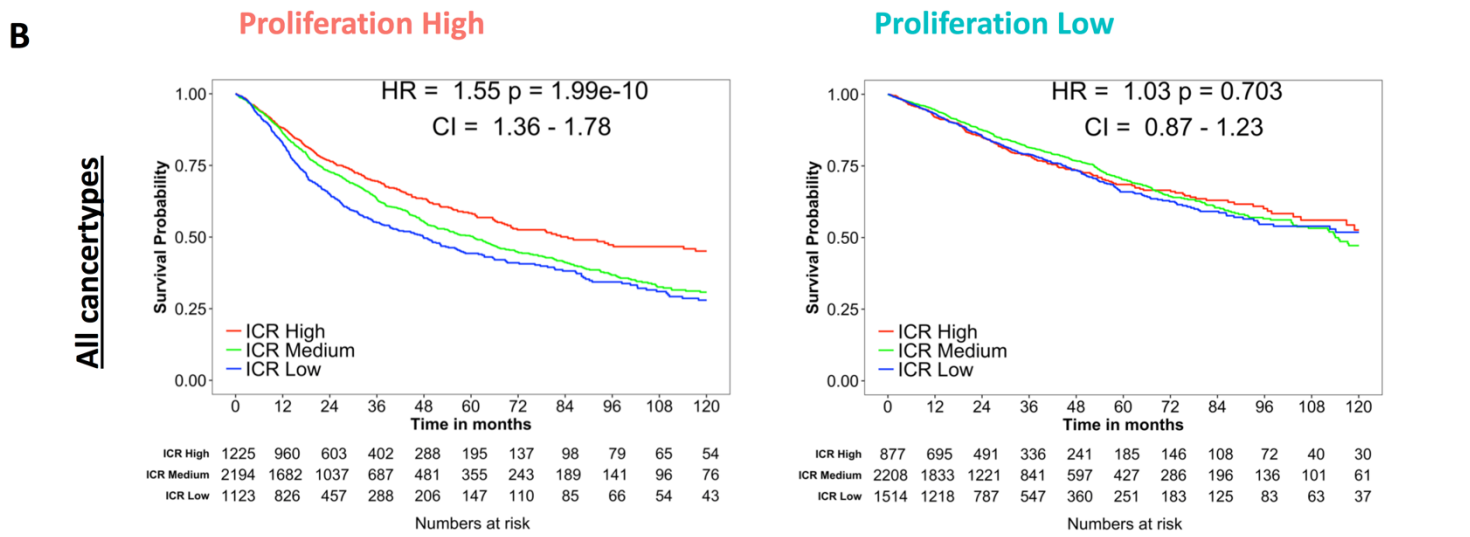
B
All cancertypes
Proliferation High
HR = 1.55 p = 1.99e-10
CI = 1.36 - 1.78
Survival Probability
1.00
0.75
0.50
0.25
0.00
ICR High
ICR Medium
ICR Low
0 12 24 36 48 60 72 84 96 108 120
Time in months
ICR High 1225 960 603 402 288 195 137 98 79 65 54
ICR Medium 2194 1682 1037 687 481 355 243 189 141 96 76
ICR Low 1123 826 457 288 206 147 110 85 66 54 43
Numbers at risk
Proliferation Low
HR = 1.03 p = 0.703
CI = 0.87 - 1.23
Survival Probability
1.00
0.75
0.50
0.25
0.00
ICR High
ICR Medium
ICR Low
0 12 24 36 48 60 72 84 96 108 120
Time in months
ICR High 877 695 491 336 241 185 146 108 72 40 30
ICR Medium 2208 1833 1221 841 597 427 286 196 136 101 61
ICR Low 1514 1218 787 547 360 251 183 125 83 63 37
Numbers at risk

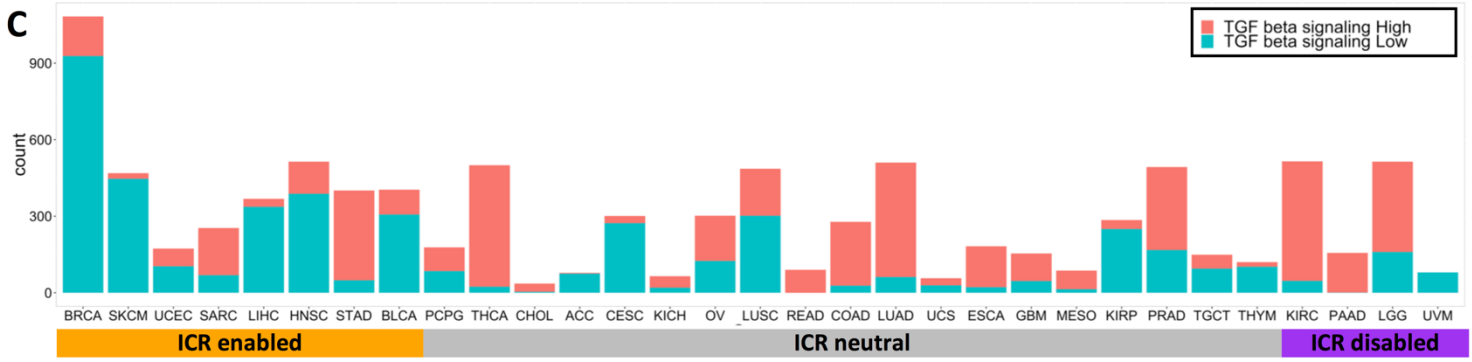
C
TGF beta signaling High
TGF beta signaling Low
count
900
600
300
0
BRCA SKCM UCEC SARC LIHC HNSC STAD BLCA PCPG THCA CHOL ACC CESC KICH OV LUSC READ COAD LUAD UCS ESCA GBM MESO KIRP PRAD TGCT THYM KIRC PAAD LGG UVM
ICR enabled
ICR neutral
ICR disabled

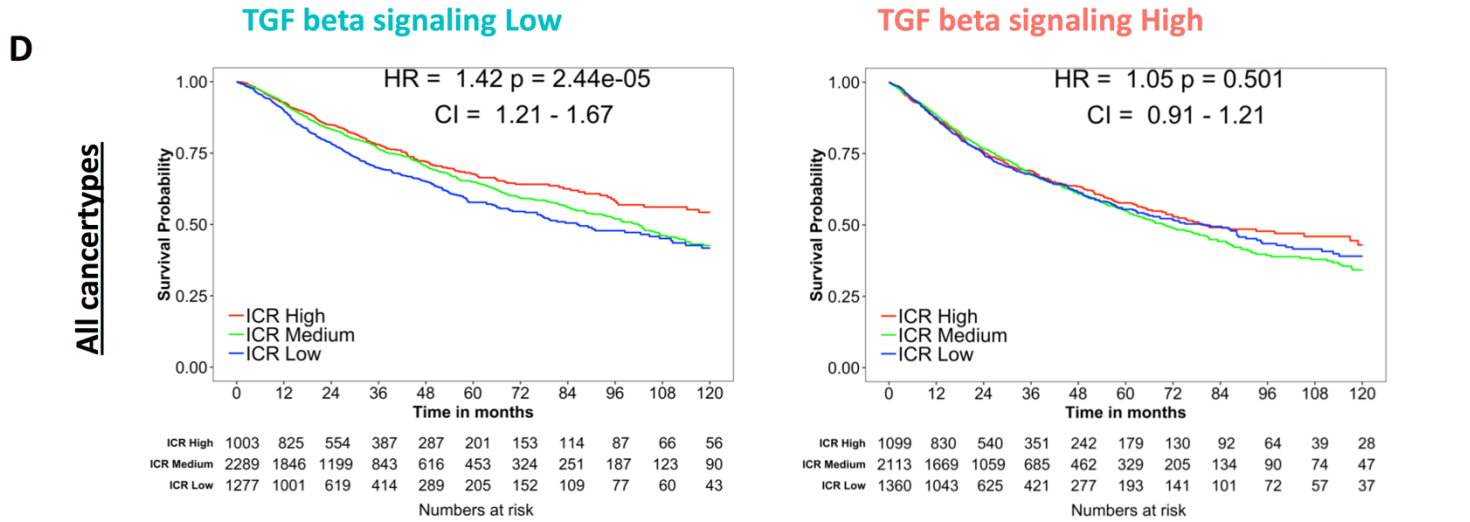
D
All cancertypes
TGF beta signaling Low
HR = 1.42 p = 2.44e-05
CI = 1.21 - 1.67
Survival Probability
1.00
0.75
0.50
0.25
0.00
ICR High
ICR Medium
ICR Low
0 12 24 36 48 60 72 84 96 108 120
Time in months
ICR High 1003 825 554 387 287 201 153 114 87 66 56
ICR Medium 2289 1846 1199 843 616 453 324 251 187 123 90
ICR Low 1277 1001 619 414 289 205 152 109 77 60 43
Numbers at risk
TGF beta signaling High
HR = 1.05 p = 0.501
CI = 0.91 - 1.21
Survival Probability
1.00
0.75
0.50
0.25
0.00
ICR High
ICR Medium
ICR Low
0 12 24 36 48 60 72 84 96 108 120
Time in months
ICR High 1099 830 540 351 242 179 130 92 64 39 28
ICR Medium 2113 1669 1059 685 462 329 205 134 90 74 47
ICR Low 1360 1043 625 421 277 193 141 101 72 57 37
Numbers at risk

387 *Predictive value of ICR score in immune checkpoint therapy is dependent on proliferation and*
388 *TGF-ß signaling*

389 To define the clinical relevance of classification of ICR immune phenotypes, in the
390 setting of immune checkpoint treatment, we first evaluated the predictive value of ICR score
391 across multiple public datasets of anti-CTLA4 and anti-PD1 treatment. A significantly
392 increased expression of ICR in responders compared to non-responders was observed across
393 most of the datasets (**Figure 7A**) (Chen et al., 2016; Hugo et al., 2016; Prat et al., 2017; Riaz
394 et al., 2017; Van Allen et al., 2015). The conditional activation of the prognostic impact of the
395 ICR was tested in the Van Allen dataset, which was the only one for which survival information
396 was available. Strikingly, in the proliferation high subgroup, ICR score was significantly higher
397 in pre-treatment samples of patients with long-survival or response (p=0.021), whereas this
398 difference was not significant in proliferation low samples (**Figure 7B**). Cohort dichotomization
399 based on TGF-ß signaling, again demonstrated the reverse trend: a significant difference in
400 ICR score was only observed in the TGF-ß signaling low group (p=0.0044), not in the TGF-ß
401 high group. Stratified survival analysis in these categories confirmed that the prognostic
402 impact of ICR depends on proliferation and TGF-ß signaling (**Figure 7C**). These findings
403 confirm a conditional prognostic and predictive impact of ICR based immune infiltration
404 estimates in the setting of immune checkpoint treatment and demonstrate that these findings
405 might have important clinical implications.

FIG7

A

Study	Platform	Treatment type	Time of biopsy	ICR score in Responders > non-responders p value
van Allen	RNASeq	anti-CTLA4	pre-treatment	0.024 (*)
Chen et al	Nanostring	anti-CTLA4	pre-treatment	0.95
		anti-CTLA4	on-treatment	0.028 (*)
		anti-PD1	pre-treatment	0.69
		anti-PD1	on-treatment	0.00054 (***)
Riaz et al (GSE91061)	RNASeq	anti-PD1	pre-treatment	0.14
		anti-PD1	on-treatment	0.015 (*)
Hugo et al (GSE78220)	RNASeq	anti-PD1	pre-treatment	0.92
Prat et al	Nanostring	anti-PD1	pre-treatment	0.05 (*)

B

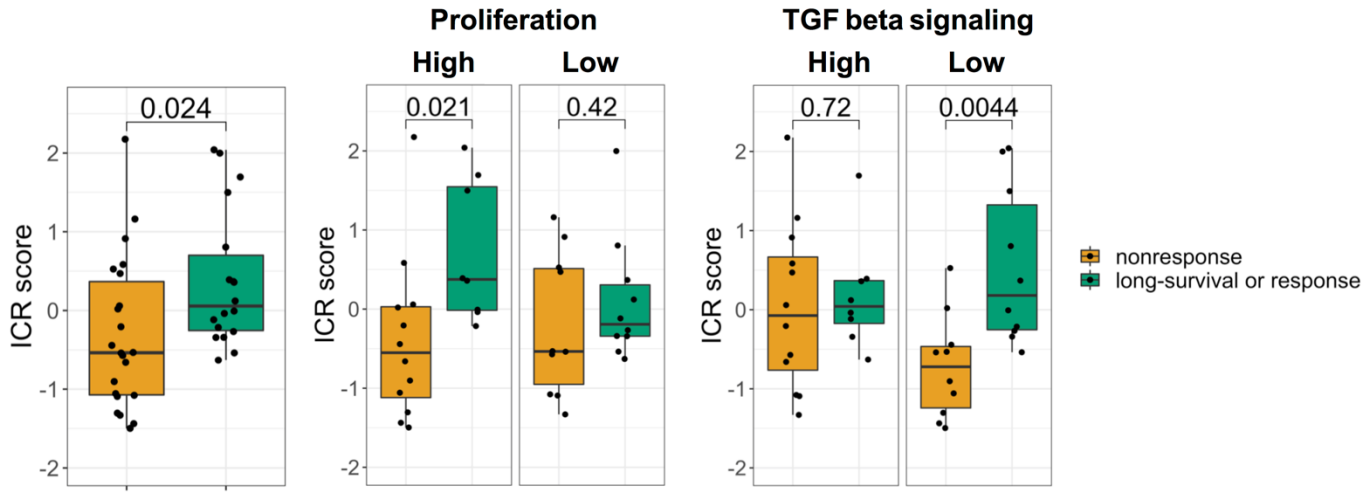

C

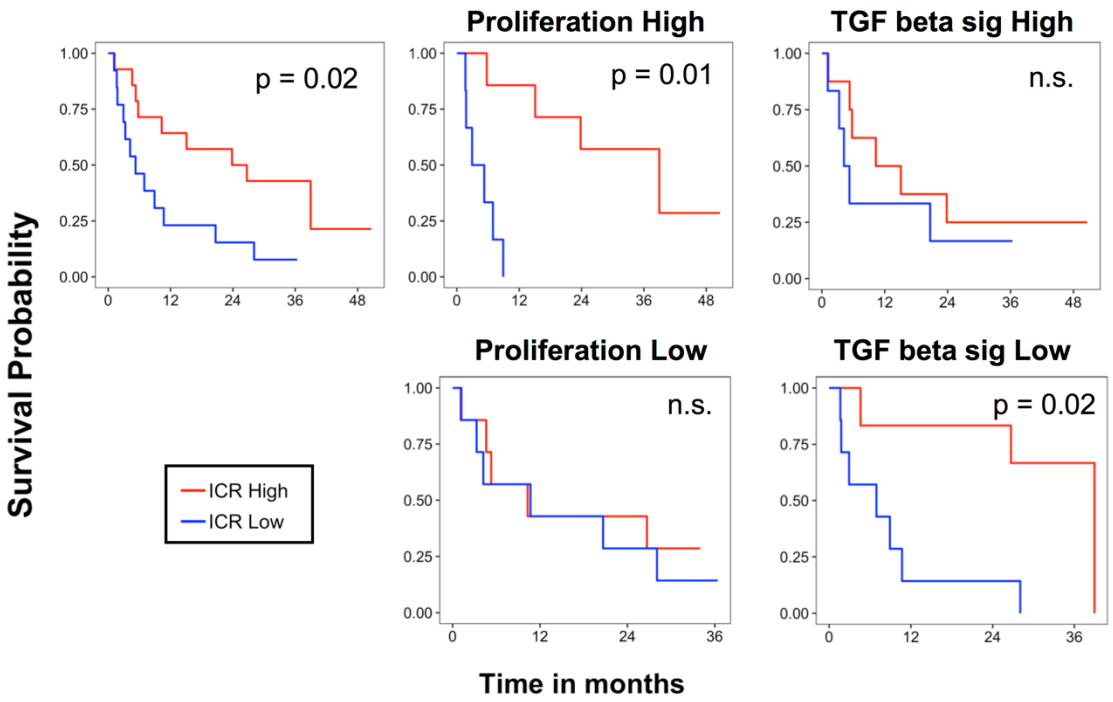

408 **Materials and Methods**

409

410 *Data acquisition and normalization*

411 RNA-seq data from The Cancer Genome Atlas (TCGA) were downloaded and processed
412 using TCGA Assembler (v2.0.3). Gene symbols were converted to official HGNC gene
413 symbols and genes without symbol or gene information were excluded. RNA-seq data from
414 as wide as possible sample set of the total of 33 available cancer types of tissue types Primary
415 Solid Tumor (TP), Recurrent Solid Tumor (TR), Additional-New Primary (TAP), Metastatic
416 (TM), Additional Metastatic (TAM) and Solid Tissue Normal (NT) were used to generate a *pan-*
417 *cancer* normalized dataset. Normalization was performed within lanes, to correct for gene-
418 specific effects (including GC-content and gene length) and between lanes, to correct for
419 sample-related differences (including sequencing depth) using R package EDASeq (v2.12.0)
420 and quantile normalized using preprocessCore (v1.36.0). After normalization, samples were
421 extracted to obtain a single primary tumor tissue (TP) sample per patient. For SKCM patients
422 without available TP sample, a metastatic sample (TM) was included. Finally, the pan-cancer
423 normalized dataset was filtered to remove duplicate patients and samples that did not pass
424 assay-specific QCs (Thorsson et al., 2018) data was log2 transformed. Clinical data were
425 sourced from the TCGA Pan-Cancer Clinical Data Resource (Liu et al., 2018). Mutation rate
426 and predicted neoantigen load were obtained from the recent immunogenomic analysis by
427 Thorsson *et al* (Thorsson et al., 2018). The dataset published by Ellrott *et al* was used for
428 mutation data analysis(Ellrott et al., 2018). Hematological cancer types LAML and DLBC were
429 excluded from analysis.

430 Raw fastq files of datasets GSE78220 (Hugo et al., 2016) and GSE78220 (Riaz et al.,
431 2017) were downloaded from NCBI SRA servers, quality control and adapter trimming was
432 performed using Trim_Galore (https://github.com/FelixKrueger/TrimGalore). Reads were
433 aligned to hg19 using STAR (Dobin et al., 2013). GenomicFeatures and GenomicAlignments
434 Bioconductor packages were used to generate row counts. The raw counts were normalized
435 with EDASeq (Risso et al., 2011) and log2 transformed. The dataset phs000452.v2.p1 (Van
436 Allen et al., 2015) was downloaded, already normalized, from http://tide.dfci.harvard.edu/.

437

438 *ICR classification*

439 Consensus clustering based on the 20 ICR genes (**Figure 1A**) was performed for each cancer
440 type separately using the ConsensusClusterPlus (v1.42.0) R package with the following
441 parameters: 5,000 repeats, a maximum of six clusters, and agglomerative hierarchical
442 clustering with ward criterion (Ward.D2) inner and complete outer linkage. The optimal number
443 of clusters ($\geq$ 3) for best segregation of samples based on the ICR signature was determined
444 heuristically using the Calinski-Harabasz criterion(Caliński and Harabasz, 1974) (source

445 function available on GitHub repository, see cancer datasheets for plots with local maximum).
446 As we were interested to compare cancer samples with a highly active immune phenotype
447 with those that have not, the cluster with the highest expression of ICR genes was designated
448 as “ICR High”, while the cluster with the lowest ICR gene expression was designated “ICR
449 Low”. All samples in intermediate cluster(s) were defined as “ICR Medium”. Samples were
450 annotated with an ICR score, defined as the mean of the normalized, log2 transformed
451 expression values of the ICR genes. For generation of the ICR Heatmaps (**Figure 1C** and the
452 cancer datasheets), a modified version of heatmap.3 function was used (source function).
453
454 *Survival analysis*
455 Overall survival (OS) from the TCGA Pan-Cancer Clinical Data Resource (Liu et al., 2018)
456 was used to generate Kaplan-Meier curves using a modified version of the ggkm function
457 (Abhijit, n.d.). Patients with less than one day of follow-up were excluded and survival data
458 were censored after a follow-up duration of 10 years. Hazard ratios (HR) between ICR Low
459 and ICR High groups, including corresponding p-values based on chi-squared test, and
460 confidence interval were calculated using the R package survival (v2.41-3). The forest plot
461 (**Figure 1C**) was generated using the R package forestplot (v1.7.2). Cancer types PCPG,
462 THYM, TGCT, and KICH were excluded before generation of the plot, as the number of deaths
463 in the comparison groups was too small for calculations. Cancer types with a HR > 1 with a p-
464 value < 0.1 were termed ICR-enabled and cancer types with a HR < 1 with a p-value < 0.1
465 were termed ICR-disabled. The forest plot was annotated manually with indicators for ICR-
466 enabled and ICR-disabled cancer types. Cox proportional hazards regression analysis was
467 performed with the R package survival with the AJCC pathologic tumor stage as described in
468 the TCGA Pan-Cancer Clinical Data Resource (Liu et al., 2018). For simplification, stage
469 categories were reduced to “Stage I”, “Stage II”, “Stage III” and “Stage IV” for subcategories
470 (e.g. Stage IIA, Stage IIB, Stage IIC etc). In multivariate analysis, pathologic stage was entered
471 as a semi-continuous (ordinal) variable. Cancer types LGG and GBM were not included in the
472 multivariate analysis as tumor stage is unavailable (not applicable) for these histologies.
473
474 *Gene Set Enrichment Analysis*
475 To define the enrichment of specific gene sets, either reflecting immune cell types (**Figure 2A**)
476 or specific oncogenic pathways (**Figure 2B**), single sample GSEA (Barbie et al., 2009) was
477 performed on the log2 transformed, normalized expression data. Immune cell-specific
478 signatures as described in Bindea *et al* (Bindea et al., 2013) were used as gene sets using
479 this method to deconvolute immune cell abundance. Gene sets to define enrichment of
480 specific tumor-related pathways were obtained from the multiple sources. We started with a
481 selection of 24 Hallmark pathways (Liberzon et al., 2015) which are regularly expressed in

482 cancer. Subsequently, we added 21 non-redundant Ingenuity Pathway Analysis (IPA)
483 pathways (http://www.ingenuity.com, Ingenuity System Inc., Redwood City, CA, USA). Finally,
484 several pathways were added that have previously been hypothesized to associate with
485 cancer immune phenotypes, including Hypoxia/Adenosine Immune Cell Suppression,
486 Immunogenic Cell Death (ICD), NOS1 Signature, PI3Kgamma signature, and SHC1/pSTAT3
487 signatures as described by Lu *et al* (Lu et al., 2017), barrier genes as described by Salerno *et*
488 *al* (Salerno et al., 2016), the proliferation metagene as described by Miller *et al* (Miller et al.,
489 2016) and genes upregulated in MAPK mutated breast cancer (Bedognetti et al., 2017).
490
491 *Correlation matrix*
492 The correlation matrices of ICR genes (**Supplementary Figure** 1) and correlation between
493 ICR score and ES of selected pathways (**Figure 2B**) were calculated using Pearson test and
494 plotted using "corrplot" version 0.84.
495
496 *Mutational Analysis*
497 Mutation rate and predicted neoantigen count data (Thorsson et al., 2018) were log10-
498 transformed and distribution across ICR clusters was plotted using R package "ggplot2".
499 Differences between ICR High, Medium and Low clusters were calculated through t-test, using
500 a cut-off p-value of < 0.05. For specific mutation analysis, a set of 470 frequently mutated
501 genes in cancer (Iorio et al., 2016), was selected. An elastic net regularized (Zou and Hastie,
502 2005) model was built to predict the ICR score as function of mutations in each sample and
503 using the tumor-type as a covariate. The accuracy of the model was evaluated in a ten-fold
504 cross-validation setting computing the correlation between the model prediction and the true
505 ICR scores, finally obtaining a Spearman correlation of 0.669 ± 0.012 (p-value $< 10^{-400}$).
506 The R package "ComplexHeatmap" was used to plot ICR score ratios between
507 mutated versus wild-type groups. For cancer type/ gene combinations with a number of
508 samples of <3 in the mutated group, ratios were not calculated (NA; grey color in plot). A ratio
509 >1 implies that the ICR score is higher in the mutated group compared with WT, while a ratio
510 <1 implies that the ICR score is higher in subset of tumors without mutation.
511
512 *Aneuploidy*
513 Aneuploidy scores for each individual cancer were taken from Taylor *et al* (Taylor et al., 2018).
514 Briefly, each tumor was scored for the presence of aneuploid chromosome arms after
515 accounting for tumor ploidy. Tumor aneuploidy scores for each cohort were then compared to
516 ICR scores via linear model with and without purity adjustment. Purity adjustment entailed
517 correlating ICR score and tumor purity (as estimated via ABSOLUTE) and using the residuals
518 to evaluate the post-adjustment relationship between ICR score and tumor aneuploidy. In

519 particular we made use of the precomputed aneuploidy scores and ABSOLUTE tumor purity
520 values. Raw ICR and aneuploidy score associations were evaluated by linear model in R via
521 the *lm()* function for each cohort independently. Adjusted ICR and aneuploidy score
522 associations were evaluated by first modeling ICR score by tumor purity, then taking the ICR
523 score residuals and assessing the association with aneuploidy score via linear model. Cohorts
524 with model p-values below 0.01 for adjusted or unadjusted ICR score and aneuploidy,
525 regardless of the directionality of the association, were included in **Figure 3C**.
526
527 *Differential GSEA and stratified survival analysis*
528 Differential ES analysis between samples of ICR-enabled and those of ICR-disabled cancer
529 types was performed using t-tests, with a cut-off of FDR-adjusted p-value (i.e., q-value) < 0.05
530 (**Supplementary Table 2**). Tumor intrinsic pathways that were differentially enriched between
531 ICR-enabled and disabled cancer types were selected. The heatmap used for visualization of
532 these differences was generated using the adapted heatmap.3 function (source function). For
533 each of these selected pathways, samples were categorized pan-cancer as pathway-High (ES
534 > median ES) or pathway-Low (ES < median ES). Associations between ICR and survival
535 were defined for each pathway "High" and pathway "Low" group separately using the survival
536 analysis methodology as described above. Pathways for which a significant association
537 between ICR and survival was present in one group, but not in the other one, were selected
538 (**Supplementary Table 3**). Similarly, these pathways were used to categorize samples per
539 individual cancer type in pathway-High (ES > cancer specific median ES) and pathway-Low
540 (ES < cancer specific median ES). Differences between HRs of groups in individual cancer
541 types were calculated and plotted using "ComplexHeatmap" (v1.17.1).
542
543 *Predictive value ICR score in immune checkpoint datasets*
544 ICR scores, or the mean expression of ICR genes, were compared between responders and
545 non-responders to immune checkpoint therapy. For the Chen et al dataset, performed on
546 Nanostring platform, scores were calculated using the 17 ICR genes available in the
547 nanostring panel. Difference in mean ICR score between groups was tested using two-side t-
548 test (cutoff <0.95) (**Fig 7A**). For datasets, GSE78220 (Riaz et al., 2017), GSE78220 (Hugo et
549 al., 2016) and Prat *et al* (Prat et al., 2017), the response category includes both partial and
550 complete clinical responders according to respective publications. For Chen et al, clinical
551 responders also included stable disease, as described by Chen *et al* (Chen et al., 2016).
552 Dataset van Allen *et al*, response was defined as patients with clinical response or long-term
553 survival after treatment (Van Allen et al., 2015). Samples of van Allen dataset were
554 dichotomized based on median ssGSEA of 1) genes of the proliferation metagene and 2) TGF-
555 ß signaling signature. Stratified analysis was performed in each of the categories. ICR High,

556 Medium and Low groups were defined according to ICR score tertiles, to obtain groups of
557 sufficient size. Stratified survival analysis was performed using the same approach as applied
558 to the TCGA data.
559
560 **Discussion**
561 Transcriptional signatures used to define the continuum of cancer immune surveillance
562 and the functional orientation of a protective anti-tumor immunity typically reflect common
563 immune processes and include largely overlapping genes (Ayers et al., 2017; Hendrickx et
564 al., 2017; Wang et al., 2008). We termed this signature as the ICR (Galon et al., 2013; Wang
565 et al., 2008).
566 In our systematic analysis we showed that, across and within different tumors, the
567 coordinated overexpression of ICR identifies a microenvironment polarized toward a Th-
568 1/cytotoxic response, which was then used to define the hot/immune active tumors.
569 In tumor types with medium/high mutational burden, the mutational or neoantigenic
570 load tended to be higher in hot (ICR high) vs cold (ICR low) tumors while this association was
571 not observed within cancer types with overall low mutational burden. By adding granularity to
572 previous observations that described an overall weak correlation between immunologic
573 correlates of anti-tumor immune response and mutational load (Danaher et al., 2018; Ock et
574 al., 2017; Rooney et al., 2015; Spranger et al., 2016; Thorsson et al., 2018), we demonstrated
575 here that the differences in term of mutational load was especially evident in tumors types
576 known to be constituted by a significant proportion of microsatellite instable cases, such as
577 COAD, STAD and UCEC. It is likely that, in hypermutated tumors, the excess of neoantigens
578 plays a major role in the immune recognition, while, in the other cases, additional mechanisms,
579 such as cell-intrinsic features, play a major role in shaping the anti-tumor immune response
580 (Hendrickx et al., 2017). Overall, a high mutational/neoantigen load was neither sufficient nor
581 necessary for the displaying of an active immune microenvironment.
582 When the ICR score was intersected with the enrichment of oncogenic signals as
583 predicted by the transcriptional data, interesting associations emerged. Although some
584 differences in terms of the degree of the correlation were observed across cancers, few tumor-
585 cell intrinsic pathways displayed a coherent progressive enrichment in the immune-silent
586 tumors. The top pathways associated with the absence of the Th1/hot immune phenotype
587 included, barriers genes, WNT-ß catenin, mismatch repair, telomerase extension by
588 telomerase, Notch, Hedgehog, and AMPK signaling pathways. Barrier genes encode for
589 molecules with mechanical barrier function in the skin and other tissues and include filaggrin
590 (FLG), tumor-associated calcium signal transducer 2 (TACSTD2), desmosomal proteins
591 (DST, DSC3, DSP, PPL, PKP3, and JUP) (Salerno et al., 2016). Their expression was
592 associated with a T-cell excluded phenotype in melanoma and ovarian cancer, and here we

593 extended our previous observation across multiple tumors (Salerno et al., 2016). The cell-
594 intrinsic WNT-ß catenin activation impairs CCL4-mediated recruitment of Batf3 dendritic cells,
595 followed by absence of CXCL10 mediated T-cell recruitment, and was described initially
596 associated with T-cell exclusion in melanoma, and recently, in other tumor types (Luke et al.,
597 2019; Spranger et al., 2015). The efficiency of our approach in capturing previously described
598 oncogenic pathways indicates the robustness of the analysis. At the same time, our integrative
599 pipeline unveiled additional relevant pathways: telomere extension by telomerase and
600 mismatch repair, Notch, Hedgehog and AMPK signaling. Our findings suggest that the lack of
601 expression of transcripts involved with mismatch repair (in addition to their genetic integrity
602 (Barnetson et al., 2006)) might influence immunogenicity. Telomere dysfunctions result in
603 various disease, including cancer and inflammatory disease (Calado and Young, 2012). To
604 our knowledge, this is the first time that telomerase activity has been linked to differential
605 intratumor immune response. The Notch pathway can regulate several target genes controlled
606 by the NFκB, TGF-β, mTORC2, PI3K, and HIF1α pathways (Janghorban et al., 2018) and is
607 involved in the induction of cancer stem cells, but has not been described to be associated
608 with differential intratumoral immune response so far. As for the Hedgehog pathway, in breast
609 cancer models, inhibition of this signaling induces a marked reduction in immune-suppressive
610 innate and adaptive cells paralleled with an enrichment of cytotoxic immune cells (Hanna et
611 al., 2019). Intriguingly, the AMPK pathway was the most coherently dysregulated pathway in
612 relationship to the ICR score. In lung cancer mouse models, the deletion of LKB1 (an upstream
613 modulator of AMPK pathway) was associated with decrease T cell tumor infiltration, and
614 impaired production of pro-inflammatory cytokines, which was mediated by induction of
615 STAT3 and IL-6 secretion (Koyama et al., 2016; Spranger and Gajewski, 2018). The strength
616 of the inverse association between the AMPK pathway and ICR score strongly calls for in-
617 depth investigation of the immune-modulatory role of this pathway. Overall, we identified novel
618 putative hierarchically relevant cancer-cell intrinsic pathways associated with immune evasion
619 mechanisms in humans that might warrant further mechanistic investigations and that might
620 be explored as targets for reprogramming the tumor microenvironment. The biological
621 relevance here is substantiated by the consistency of the associations across tumor types, in
622 which each cohort can be seen as an independent validation. The coherence of the
623 associations rules out the possibility of a spurious correlation.

624 As for somatic mutations, the top ten genes associated with the immune silent
625 phenotype include *IDH1, IDH2, FOXA2, NSD1, PSIP1, HDAC3, ZNF814, MAP3K1, FRG1*
626 *and SOX17.* Findings of *IDH1* and *NSD1* are consistent with the report of Thorsson et al
627 (Thorsson et al., 2018), in which these have been associated with decreased leukocyte
628 infiltration, and are complemented here by additional identification of *IDH2*. Interestingly,
629 MAP3K1 mutations were previously associated with low ICR in breast cancer in our previous

630 work (Bedognetti et al., 2017; Hendrickx et al., 2017). Remarkably, mutations of other genes
631 of the RAS/MAPK pathways such as *FGFR3* (previously associated with T-cell exclusion in
632 bladder cancer (Sweis et al., 2016)), *EGFR, NRAS,* and *KRAS* were associated with a low
633 ICR score, substantiating their potential role in mediating immune exclusion. FOXA2 is
634 involved in both neoplastic transformation and epithelial-mesenchymal transition (Wang et al.,
635 2018, p. 2) and T helper differentiation (Chen et al., 2010) but its role in modulating anti-tumor
636 immune response is unknown. Similarly, no data exists on the effect of *HDAC3, PSIP1* and
637 *ZNF814* on tumor immunogenicity. Considering the strength of the association, further
638 investigations should mechanistically address the role of these signaling pathways in
639 mediating immune evasion mechanisms. Other mutations associated with the immune silent
640 phenotype include *WNT5A* (corroborating the immune-suppressive role of the WNT ß catenin
641 pathway (Luke et al., 2019)), and *GATA3*, which was also previously associated with low
642 leukocyte infiltration (Thorsson et al., 2018). Mutations of *FKBP5*, *MAT2A, PPP2R5A,*
643 *MECOM, SMAD2, MED17, ADAM10, PRKAR1A, DIS3, PRRX1, MFNG, TNPO1, KDM6A,*
644 *IRF7, SUZ12*, *RPSAP58*, and *SF3B1* represent additional novel findings. Similar to previous
645 observations, we found *HLA-A*, *HLA-B*, *B2M*, *CASP8* and *FAS* to be associated with an ICR
646 High immune phenotype (Ock et al., 2017; Rooney et al., 2015; Shukla et al., 2015; Siemers
647 et al., 2017; Thorsson et al., 2018). These mutations are probably the result of immune escape
648 mechanisms triggered by immunologic pressure.

649 As for genomic instability, tumors with high aneuploidy are associated with decreased
650 ICR score in a major subset of cancer types (Davoli et al., 2017). This observation is also in
651 agreement with negative association of a chromosome-instable type with an immune
652 signature that predicts response to immunotherapy with MAGE-A3 antigen as well as
653 response to anti-CTLA-4 treatment in melanoma (Ock et al., 2017). The only exceptions we
654 found were brain tumors LGG and GBM in which a positive association between aneuploidy
655 and ICR score was detected. In LGG tumors, however, ICR scores positively correlate with
656 tumor grade (**Supplementary Figure 4**), and it is possible that the observed positive
657 correlation between aneuploidy and ICR is actually driven by the higher genomic instability
658 characterizing the more advanced tumors.

659 To compare cancer types based on the prognostic value of ICR, we categorized them
660 into two groups: one for which ICR High was associated with increased OS and one for which
661 ICR was associated with worse OS. For the first group, multivariate analysis confirmed a
662 positive prognostic value of ICR independent of pathologic tumor stage. SKCM, BRCA, UCEC,
663 LIHC, SARC, HNSC, STAD, and BLCA are consequently referred to as **ICR-enabled** cancer
664 types. For the second group, including UVM, LGG, PAAD, and KIRC (**ICR-disabled** tumors),
665 survival analysis showed a detrimental (univariate analysis) or neutral (multivariate analysis
666 with stage) role of ICR.

667 These discrepancies in term of prognostic implication of intratumoral immune
668 response have been observed in independent investigations based on transcriptomic analysis
669 (Chifman et al., 2016; Thorsson et al., 2018) or immunohistochemistry (Fridman et al., 2012)
670 but never explained.
671 The first notable difference we observed between ICR-enabled and -disabled cancer
672 types was the overall lower ICR value in the disabled cancer cohorts. In particular for UVM
673 and LGG, this low ICR could be a partial explanation for the lack of positive prognostic value
674 of the ICR. On the other hand, mean ICR score of PAAD and KIRC was not different compared
675 with the other cancer types. Therefore, other factors must have an effect on the prognostic
676 value of the ICR. When we compared enrichment of tumor-cell intrinsic pathways in ICR-
677 enabled and -disabled cancer types, as much as 43 of 54 analyzed pathways showed
678 differential enrichment between the two groups. While ICR-enabled cancer types are typically
679 more enriched in proliferation-related signatures, ICR-disabled cancer types have high
680 enrichment of pathways generally attributed to tumor signaling including known pathways
681 associated with immune suppression such as TGF-ß (Chakravarthy et al., 2018). In fact, when
682 samples of the entire cohort were segregated according to representative enabling and
683 disabling pathways (i.e., proliferation and TGF-ß signaling, respectively), the prognostic role
684 of ICR was restricted to proliferation high/TGF-ß signaling low tumors (**Figure 6**). Hierarchical
685 clustering based on the enrichment of transcripts of these differentially enriched pathways
686 segregated most samples of ICR-enabled cancer types from samples of ICR-disabled cancer
687 types. Interestingly, this clustering was even relevant to samples of ICR neutral cancer types.
688 The pan-cancer survival analysis of samples of ICR neutral cancer types showed that for
689 samples that co-clustered with samples of ICR-enabled cancer types (the ICR beneficial
690 cluster), ICR High was associated with significant prolonged survival. Conversely, in samples
691 of ICR neutral cancer types clustered to the ICR non-beneficial cluster, ICR lost its prognostic
692 value. Adding the mutational load component further refined this stratification. In fact, the
693 positive prognostic role of ICR was present also in a subset of samples with low proliferation
694 and high mutational load but absent only in tumors with both low proliferation and low
695 mutational load. We hypothesize that, in tumor with high mutational burden and/or high
696 proliferative capacity, the high level of ICR captures a true protective anti-tumoral immune
697 response, while in the other cases, such as in tumors dominated by TGF-ß signaling and low
698 proliferation, the high ICR captures a bystander, or heavily suppressed, lymphocyte infiltration
699 with no protective effect. Therefore, it is possible to speculate that a proportion of
700 phenotypically immune active tumors are functionally immune silent. Single cell RNA
701 sequencing, T-cell receptor sequencing, and spatial transcriptional analysis might be
702 employed to characterize with higher fidelity the true functional orientation of human tumors.

703 The clinical relevance of the observed conditional impact of ICR was confirmed in the
704 setting of anti-CTLA4 treatment, in which the predictive value of ICR was demonstrated to be
705 dependent on tumor intrinsic pathways, such as TGF-ß and proliferation. To the best of our
706 knowledge, we are the first to report an interaction between tumor intrinsic pathways and the
707 prognostic value of immune phenotypes in a pan-cancer analysis. An association between
708 proliferation and the prognostic value of immune phenotypes has previously been identified in
709 breast cancer (Miller et al., 2016). In non-small cell lung cancer, proliferation was shown to
710 improve prediction of immune checkpoint inhibitors response in PD-L1 positive samples (data
711 recently presented at SITC annual meeting 2018 ("SITC 2018 Annual Meeting Schedule,"
712 n.d.)). Our study clearly demonstrates that such interactions between tumor intrinsic attributes
713 and prognostic and potentially predictive value of immune phenotypes are also relevant in a
714 pan-cancer context. Moreover, we defined additional tumor intrinsic attributes beyond tumor
715 proliferation to correlate with the prognostic significance of immune signatures reflecting a Th1
716 immune response. Prognostication algorithms should be refined by inclusion of tumor intrinsic
717 attributes in order to define the prognostic impact of the immune signatures.
718 In conclusion, we observed a clear relationship between enrichment of tumor intrinsic
719 pathways and the prognostic and predictive significance of the immune signatures and
720 identified novel cell-intrinsic features associated with immune exclusion. This information can
721 be used to prioritize candidates for immunogenic conversion and to refine stratification
722 algorithms.

723 **References**

724 Abhijit. n.d. An enhanced Kaplan-Meier plot. *Stat Bandit*.
725 Ayers M, Lunceford J, Nebozhyn M, Murphy E, Loboda A, Kaufman DR, Albright A, Cheng
726 JD, Kang SP, Shankaran V, Piha-Paul SA, Yearley J, Seiwert TY, Ribas A,
727 McClanahan TK. 2017. IFN-γ-related mRNA profile predicts clinical response to PD-1
728 blockade. *J Clin Invest* 127:2930–2940. doi:10.1172/JCI91190
729 Barbie DA, Tamayo P, Boehm JS, Kim SY, Moody SE, Dunn IF, Schinzel AC, Sandy P,
730 Meylan E, Scholl C, Fröhling S, Chan EM, Sos ML, Michel K, Mermel C, Silver SJ,
731 Weir BA, Reiling JH, Sheng Q, Gupta PB, Wadlow RC, Le H, Hoersch S, Wittner BS,
732 Ramaswamy S, Livingston DM, Sabatini DM, Meyerson M, Thomas RK, Lander ES,
733 Mesirov JP, Root DE, Gilliland DG, Jacks T, Hahn WC. 2009. Systematic RNA
734 interference reveals that oncogenic KRAS-driven cancers require TBK1. *Nature*
735 462:108–112. doi:10.1038/nature08460
736 Barnetson RA, Tenesa A, Farrington SM, Nicholl ID, Cetnarskyj R, Porteous ME, Campbell
737 H, Dunlop MG. 2006. Identification and Survival of Carriers of Mutations in DNA
738 Mismatch-Repair Genes in Colon Cancer. *N Engl J Med* 354:2751–2763.
739 doi:10.1056/NEJMoa053493
740 Bedognetti D, Hendrickx W, Ceccarelli M, Miller LD, Seliger B. 2016. Disentangling the
741 relationship between tumor genetic programs and immune responsiveness. *Curr*
742 *Opin Immunol*, Lymphocyte development and activation * Tumour immunology
743 39:150–158. doi:10.1016/j.coi.2016.02.001
744 Bedognetti D, Roelands J, Decock J, Wang E, Hendrickx W. 2017. The MAPK hypothesis:
745 immune-regulatory effects of MAPK-pathway genetic dysregulations and implications
746 for breast cancer immunotherapy. *Emerg Top Life Sci* 1:429–445.
747 doi:10.1042/ETLS20170142
748 Bedognetti D, Spivey TL, Zhao Y, Uccellini L, Tomei S, Dudley ME, Ascierto ML, De Giorgi
749 V, Liu Q, Delogu LG, Sommariva M, Sertoli MR, Simon R, Wang E, Rosenberg SA,
750 Marincola FM. 2013. CXCR3/CCR5 pathways in metastatic melanoma patients
751 treated with adoptive therapy and interleukin-2. *Br J Cancer* 109:2412–2423.
752 doi:10.1038/bjc.2013.557
753 Bertucci F, Finetti P, Simeone I, Hendrickx W, Wang E, Marincola FM, Viens P, Mamessier
754 E, Ceccarelli M, Birnbaum D, Bedognetti D. 2018. The immunologic constant of
755 rejection classification refines the prognostic value of conventional prognostic
756 signatures in breast cancer. *Br J Cancer*. doi:10.1038/s41416-018-0309-1
757 Bindea G, Mlecnik B, Tosolini M, Kirilovsky A, Waldner M, Obenauf AC, Angell H, Fredriksen
758 T, Lafontaine L, Berger A, Bruneval P, Fridman WH, Becker C, Pagès F, Speicher
759 MR, Trajanoski Z, Galon J. 2013. Spatiotemporal dynamics of intratumoral immune
760 cells reveal the immune landscape in human cancer. *Immunity* 39:782–795.
761 doi:10.1016/j.immuni.2013.10.003
762 Calado R, Young N. 2012. Telomeres in disease. *F1000 Med Rep* 4:8. doi:10.3410/M4-8
763 Caliński T, Harabasz J. 1974. A dendrite method for cluster analysis. *Commun Stat* 3:1–27.
764 doi:10.1080/03610927408827101
765 Chakravarthy A, Khan L, Bensler NP, Bose P, Carvalho DDD. 2018. TGF-β-associated
766 extracellular matrix genes link cancer-associated fibroblasts to immune evasion and
767 immunotherapy failure. *Nat Commun* 9:4692. doi:10.1038/s41467-018-06654-8
768 Charoentong P, Finotello F, Angelova M, Mayer C, Efremova M, Rieder D, Hackl H,
769 Trajanoski Z. 2017. Pan-cancer Immunogenomic Analyses Reveal Genotype-
770 Immunophenotype Relationships and Predictors of Response to Checkpoint
771 Blockade. *Cell Rep* 18:248–262. doi:10.1016/j.celrep.2016.12.019
772 Chen G, Wan H, Luo F, Zhang L, Xu Y, Lewkowich I, Wills-Karp M, Whitsett JA. 2010.
773 Foxa2 programs Th2 cell-mediated innate immunity in the developing lung. *J*
774 *Immunol Baltim Md 1950* 184:6133–6141. doi:10.4049/jimmunol.1000223
775 Chen P-L, Roh W, Reuben A, Cooper ZA, Spencer CN, Prieto PA, Miller JP, Bassett RL,
776 Gopalakrishnan V, Wani K, De Macedo MP, Austin-Breneman JL, Jiang H, Chang Q,

Reddy SM, Chen W-S, Tetzlaff MT, Broaddus RJ, Davies MA, Gershenwald JE, Haydu L, Lazar AJ, Patel SP, Hwu P, Hwu W-J, Diab A, Glitza IC, Woodman SE, Vence LM, Wistuba II, Amaria RN, Kwong LN, Prieto V, Davis RE, Ma W, Overwijk WW, Sharpe AH, Hu J, Futreal PA, Blando J, Sharma P, Allison JP, Chin L, Wargo JA. 2016. Analysis of Immune Signatures in Longitudinal Tumor Samples Yields Insight into Biomarkers of Response and Mechanisms of Resistance to Immune Checkpoint Blockade. *Cancer Discov* 6:827–837. doi:10.1158/2159-8290.CD-15-1545

Chifman J, Pullikuth A, Chou JW, Bedognetti D, Miller LD. 2016. Conservation of immune gene signatures in solid tumors and prognostic implications. *BMC Cancer* 16:911. doi:10.1186/s12885-016-2948-z

Corrales L, Matson V, Flood B, Spranger S, Gajewski TF. 2017. Innate immune signaling and regulation in cancer immunotherapy. *Cell Res* 27:96–108. doi:10.1038/cr.2016.149

Cortes-Ciriano I, Lee S, Park W-Y, Kim T-M, Park PJ. 2017. A molecular portrait of microsatellite instability across multiple cancers. *Nat Commun* 8. doi:10.1038/ncomms15180

Danaher P, Warren S, Lu R, Samayoa J, Sullivan A, Pekker I, Wallden B, Marincola FM, Cesano A. 2018. Pan-cancer adaptive immune resistance as defined by the Tumor Inflammation Signature (TIS): results from The Cancer Genome Atlas (TCGA). *J Immunother Cancer* 6:63. doi:10.1186/s40425-018-0367-1

Dandapani M, Hardie DG. 2013. AMPK: opposing the metabolic changes in both tumour cells and inflammatory cells? *Biochem Soc Trans* 41:687–693. doi:10.1042/BST20120351

Davoli T, Uno H, Wooten EC, Elledge SJ. 2017. Tumor aneuploidy correlates with markers of immune evasion and with reduced response to immunotherapy. *Science* 355:eaaf8399. doi:10.1126/science.aaf8399

Dobin A, Davis CA, Schlesinger F, Drenkow J, Zaleski C, Jha S, Batut P, Chaisson M, Gingeras TR. 2013. STAR: ultrafast universal RNA-seq aligner. *Bioinforma Oxf Engl* 29:15–21. doi:10.1093/bioinformatics/bts635

Economopoulou P, Perisanidis C, Giotakis EI, Psyrri A. 2016. The emerging role of immunotherapy in head and neck squamous cell carcinoma (HNSCC): anti-tumor immunity and clinical applications. *Ann Transl Med* 4. doi:10.21037/atm.2016.03.34

Ellrott K, Bailey MH, Saksena G, Covington KR, Kandoth C, Stewart C, Hess J, Ma S, Chiotti KE, McLellan M, Sofia HJ, Hutter C, Getz G, Wheeler D, Ding L, MC3 Working Group, Cancer Genome Atlas Research Network. 2018. Scalable Open Science Approach for Mutation Calling of Tumor Exomes Using Multiple Genomic Pipelines. *Cell Syst* 6:271-281.e7. doi:10.1016/j.cels.2018.03.002

Emens LA, Ascierto PA, Darcy PK, Demaria S, Eggermont AMM, Redmond WL, Seliger B, Marincola FM. 2017. Cancer immunotherapy: Opportunities and challenges in the rapidly evolving clinical landscape. *Eur J Cancer Oxf Engl 1990* 81:116–129. doi:10.1016/j.ejca.2017.01.035

Fridman WH, Pagès F, Sautès-Fridman C, Galon J. 2012. The immune contexture in human tumours: impact on clinical outcome. *Nat Rev Cancer* 12:298–306. doi:10.1038/nrc3245

Galon J, Angell HK, Bedognetti D, Marincola FM. 2013. The Continuum of Cancer Immunosurveillance: Prognostic, Predictive, and Mechanistic Signatures. *Immunity* 39:11–26. doi:10.1016/j.immuni.2013.07.008

Gong J, Chehrazi-Raffle A, Reddi S, Salgia R. 2018. Development of PD-1 and PD-L1 inhibitors as a form of cancer immunotherapy: a comprehensive review of registration trials and future considerations. *J Immunother Cancer* 6:8. doi:10.1186/s40425-018-0316-z

Hanna A, Metge BJ, Bailey SK, Chen D, Chandrashekar DS, Varambally S, Samant RS, Shevde LA. 2019. Inhibition of Hedgehog signaling reprograms the dysfunctional

831 immune microenvironment in breast cancer. *Oncoimmunology* 8:1548241.
832 doi:10.1080/2162402X.2018.1548241
833 Hendrickx W, Simeone I, Anjum S, Mokrab Y, Bertucci F, Finetti P, Curigliano G, Seliger B,
834 Cerulo L, Tomei S, Delogu LG, Maccalli C, Wang E, Miller LD, Marincola FM,
835 Ceccarelli M, Bedognetti D. 2017. Identification of genetic determinants of breast
836 cancer immune phenotypes by integrative genome-scale analysis. *OncoImmunology*
837 0:00–00. doi:10.1080/2162402X.2016.1253654
838 Hugo W, Zaretsky JM, Sun L, Song C, Moreno BH, Hu-Lieskovan S, Berent-Maoz B, Pang
839 J, Chmielowski B, Cherry G, Seja E, Lomeli S, Kong X, Kelley MC, Sosman JA,
840 Johnson DB, Ribas A, Lo RS. 2016. Genomic and Transcriptomic Features of
841 Response to Anti-PD-1 Therapy in Metastatic Melanoma. *Cell* 165:35–44.
842 doi:10.1016/j.cell.2016.02.065
843 Iorio F, Knijnenburg TA, Vis DJ, Bignell GR, Menden MP, Schubert M, Aben N, Gonçalves
844 E, Barthorpe S, Lightfoot H, Cokelaer T, Greninger P, Dyk E van, Chang H, Silva H
845 de, Heyn H, Deng X, Egan RK, Liu Q, Mironenko T, Mitropoulos X, Richardson L,
846 Wang J, Zhang T, Moran S, Sayols S, Soleimani M, Tamborero D, Lopez-Bigas N,
847 Ross-Macdonald P, Esteller M, Gray NS, Haber DA, Stratton MR, Benes CH,
848 Wessels LFA, Saez-Rodriguez J, McDermott U, Garnett MJ. 2016. A Landscape of
849 Pharmacogenomic Interactions in Cancer. *Cell* 166:740–754.
850 doi:10.1016/j.cell.2016.06.017
851 Janghorban M, Xin L, Rosen JM, Zhang XH-F. 2018. Notch Signaling as a Regulator of the
852 Tumor Immune Response: To Target or Not To Target? *Front Immunol* 9.
853 doi:10.3389/fimmu.2018.01649
854 Koyama S, Akbay EA, Li YY, Aref AR, Skoulidis F, Herter-Sprie GS, Buczkowski KA, Liu Y,
855 Awad MM, Denning WL, Diao L, Wang J, Parra-Cuentas ER, Wistuba II, Soucheray
856 M, Thai T, Asahina H, Kitajima S, Altabef A, Cavanaugh JD, Rhee K, Gao P, Zhang
857 H, Fecci PE, Shimamura T, Hellmann MD, Heymach JV, Hodi FS, Freeman GJ,
858 Barbie DA, Dranoff G, Hammerman PS, Wong K-K. 2016. STK11/LKB1 Deficiency
859 Promotes Neutrophil Recruitment and Proinflammatory Cytokine Production to
860 Suppress T-cell Activity in the Lung Tumor Microenvironment. *Cancer Res* 76:999–
861 1008. doi:10.1158/0008-5472.CAN-15-1439
862 Liberzon A, Birger C, Thorvaldsdóttir H, Ghandi M, Mesirov JP, Tamayo P. 2015. The
863 Molecular Signatures Database Hallmark Gene Set Collection. *Cell Syst* 1:417–425.
864 doi:10.1016/j.cels.2015.12.004
865 Liu J, Lichtenberg T, Hoadley KA, Poisson LM, Lazar AJ, Cherniack AD, Kovatich AJ, Benz
866 CC, Levine DA, Lee AV, Omberg L, Wolf DM, Shriver CD, Thorsson V, Cancer
867 Genome Atlas Research Network, Hu H. 2018. An Integrated TCGA Pan-Cancer
868 Clinical Data Resource to Drive High-Quality Survival Outcome Analytics. *Cell*
869 173:400-416.e11. doi:10.1016/j.cell.2018.02.052
870 Lu R, Turan T, Samayoa J, Marincola FM. 2017. Cancer immune resistance: can theories
871 converge? *Emerg Top Life Sci* 1:411–419. doi:10.1042/ETLS20170060
872 Luke JJ, Bao R, Sweis RF, Spranger S, Gajewski TF. 2019. WNT/β-catenin pathway
873 activation correlates with immune exclusion across human cancers. *Clin Cancer Res*
874 *Off J Am Assoc Cancer Res*. doi:10.1158/1078-0432.CCR-18-1942
875 McGranahan T, Li G, Nagpal S. 2017. History and current state of immunotherapy in glioma
876 and brain metastasis. *Ther Adv Med Oncol* 9:347–368.
877 doi:10.1177/1758834017693750
878 Miller LD, Chou JA, Black MA, Print C, Chifman J, Alistar A, Putti T, Zhou X, Bedognetti D,
879 Hendrickx W, Pullikuth A, Rennhack J, Andrechek ER, Demaria S, Wang E,
880 Marincola FM. 2016. Immunogenic Subtypes of Breast Cancer Delineated by Gene
881 Classifiers of Immune Responsiveness. *Cancer Immunol Res*. doi:10.1158/2326-
882 6066.CIR-15-0149
883 Nagalla S, Chou JW, Willingham MC, Ruiz J, Vaughn JP, Dubey P, Lash TL, Hamilton-
884 Dutoit SJ, Bergh J, Sotiriou C, Black MA, Miller LD. 2013. Interactions between

885 immunity, proliferation and molecular subtype in breast cancer prognosis. *Genome*
886 *Biol* 14:R34. doi:10.1186/gb-2013-14-4-r34
887 Ock C-Y, Hwang J-E, Keam B, Kim S-B, Shim J-J, Jang H-J, Park S, Sohn BH, Cha M, Ajani
888 JA, Kopetz S, Lee K-W, Kim TM, Heo DS, Lee J-S. 2017. Genomic landscape
889 associated with potential response to anti-CTLA-4 treatment in cancers. *Nat*
890 *Commun* 8:1050. doi:10.1038/s41467-017-01018-0
891 Passarelli A, Mannavola F, Stucci LS, Tucci M, Silvestris F. 2017. Immune system and
892 melanoma biology: a balance between immunosurveillance and immune escape.
893 *Oncotarget* 8:106132–106142. doi:10.18632/oncotarget.22190
894 Prat A, Navarro A, Paré L, Reguart N, Galvan P, Pascual T, Martínez A, Nuciforo P,
895 Comerma L, Alos L, Pardo N, Cedrés S, Fan C, Parker JS, Gaba L, Victoria I,
896 Viñolas N, Vivancos A, Arance A, Felip E. 2017. Immune-related gene expression
897 profiling after PD-1 blockade in non-small cell lung carcinoma, head and neck
898 squamous cell carcinoma and melanoma. *Cancer Res* canres.3556.2017.
899 doi:10.1158/0008-5472.CAN-16-3556
900 Riaz N, Havel JJ, Makarov V, Desrichard A, Urba WJ, Sims JS, Hodi FS, Martín-Algarra S,
901 Mandal R, Sharfman WH, Bhatia S, Hwu W-J, Gajewski TF, Slingluff CL, Chowell D,
902 Kendall SM, Chang H, Shah R, Kuo F, Morris LGT, Sidhom J-W, Schneck JP, Horak
903 CE, Weinhold N, Chan TA. 2017. Tumor and Microenvironment Evolution during
904 Immunotherapy with Nivolumab. *Cell*. doi:10.1016/j.cell.2017.09.028
905 Risso D, Schwartz K, Sherlock G, Dudoit S. 2011. GC-Content Normalization for RNA-Seq
906 Data. *BMC Bioinformatics* 12:480. doi:10.1186/1471-2105-12-480
907 Rooney MS, Shukla SA, Wu CJ, Getz G, Hacohen N. 2015. Molecular and Genetic
908 Properties of Tumors Associated with Local Immune Cytolytic Activity. *Cell* 160:48–
909 61. doi:10.1016/j.cell.2014.12.033
910 Salerno EP, Bedognetti D, Mauldin IS, Deacon DH, Shea SM, Pinczewski J, Obeid JM,
911 Coukos G, Wang E, Gajewski TF, Marincola FM, Slingluff CL. 2016. Human
912 melanomas and ovarian cancers overexpressing mechanical barrier molecule genes
913 lack immune signatures and have increased patient mortality risk. *OncoImmunology*
914 5:e1240857. doi:10.1080/2162402X.2016.1240857
915 Shukla SA, Rooney MS, Rajasagi M, Tiao G, Dixon PM, Lawrence MS, Stevens J, Lane WJ,
916 Dellagatta JL, Steelman S, Sougnez C, Cibulskis K, Kiezun A, Hacohen N, Brusic V,
917 Wu CJ, Getz G. 2015. Comprehensive analysis of cancer-associated somatic
918 mutations in class I HLA genes. *Nat Biotechnol* 33:1152–1158. doi:10.1038/nbt.3344
919 Siemers NO, Holloway JL, Chang H, Chasalow SD, Ross-MacDonald PB, Voliva CF,
920 Szustakowski JD. 2017. Genome-wide association analysis identifies genetic
921 correlates of immune infiltrates in solid tumors. *PLoS ONE* 12.
922 doi:10.1371/journal.pone.0179726
923 SITC 2018 Annual Meeting Schedule. n.d. https://www.sitcancer.org/2018/schedule
924 Spranger S, Bao R, Gajewski TF. 2015. Melanoma-intrinsic β-catenin signalling prevents
925 anti-tumour immunity. *Nature* 523:231–235. doi:10.1038/nature14404
926 Spranger S, Gajewski TF. 2018. Impact of oncogenic pathways on evasion of antitumour
927 immune responses. *Nat Rev Cancer* 18:139–147. doi:10.1038/nrc.2017.117
928 Spranger S, Gajewski TF. 2015. Tumor-intrinsic oncogene pathways mediating immune
929 avoidance. *Oncoimmunology* 5. doi:10.1080/2162402X.2015.1086862
930 Spranger S, Luke JJ, Bao R, Zha Y, Hernandez KM, Li Y, Gajewski AP, Andrade J,
931 Gajewski TF. 2016. Density of immunogenic antigens does not explain the presence
932 or absence of the T-cell-inflamed tumor microenvironment in melanoma. *Proc Natl*
933 *Acad Sci U S A* 113:E7759–E7768. doi:10.1073/pnas.1609376113
934 Sweis RF, Spranger S, Bao R, Paner GP, Stadler WM, Steinberg G, Gajewski TF. 2016.
935 Molecular Drivers of the Non-T-cell-Inflamed Tumor Microenvironment in Urothelial
936 Bladder Cancer. *Cancer Immunol Res* 4:563–568. doi:10.1158/2326-6066.CIR-15-
937 0274
938 Tamborero D, Rubio-Perez C, Muiños F, Sabarinathan R, Piulats JM, Muntasell A,
939 Dienstmann R, Lopez-Bigas N, Gonzalez-Perez A. 2018. A pan-cancer landscape of

940 interactions between solid tumors and infiltrating immune cell populations. *Clin*
941 *Cancer Res* clincanres.3509.2017. doi:10.1158/1078-0432.CCR-17-3509
942 Taylor AM, Shih J, Ha G, Gao GF, Zhang X, Berger AC, Schumacher SE, Wang C, Hu H,
943 Liu Jianfang, Lazar AJ, Caesar-Johnson SJ, Demchok JA, Felau I, Kasapi M,
944 Ferguson ML, Hutter CM, Sofia HJ, Tarnuzzer R, Wang Z, Yang L, Zenklusen JC,
945 Zhang J (Julia), Chudamani S, Liu Jia, Lolla L, Naresh R, Pihl T, Sun Q, Wan Y, Wu
946 Y, Cho J, DeFreitas T, Frazer S, Gehlenborg N, Getz G, Heiman DI, Kim J,
947 Lawrence MS, Lin P, Meier S, Noble MS, Saksena G, Voet D, Zhang Hailei, Bernard
948 B, Chambwe N, Dhankani V, Knijnenburg T, Kramer R, Leinonen K, Liu Y, Miller M,
949 Reynolds S, Shmulevich I, Thorsson V, Zhang W, Akbani R, Broom BM, Hegde AM,
950 Ju Z, Kanchi RS, Korkut A, Li J, Liang H, Ling S, Liu W, Lu Y, Mills GB, Ng K-S, Rao
951 A, Ryan M, Wang Jing, Weinstein JN, Zhang J, Abeshouse A, Armenia J,
952 Chakravarty D, Chatila WK, Bruijn I de, Gao J, Gross BE, Heins ZJ, Kundra R, La K,
953 Ladanyi M, Luna A, Nissan MG, Ochoa A, Phillips SM, Reznik E, Sanchez-Vega F,
954 Sander C, Schultz N, Sheridan R, Sumer SO, Sun Y, Taylor BS, Wang Jioajiao,
955 Zhang Hongxin, Anur P, Peto M, Spellman P, Benz C, Stuart JM, Wong CK, Yau C,
956 Hayes DN, Parker JS, Wilkerson MD, Ally A, Balasundaram M, Bowlby R, Brooks D,
957 Carlsen R, Chuah E, Dhalla N, Holt R, Jones SJM, Kasaian K, Lee D, Ma Y, Marra
958 MA, Mayo M, Moore RA, Mungall AJ, Mungall K, Robertson AG, Sadeghi S, Schein
959 JE, Sipahimalani P, Tam A, Thiessen N, Tse K, Wong T, Berger AC, Beroukhim R,
960 Cherniack AD, Cibulskis C, Gabriel SB, Gao GF, Ha G, Meyerson M, Schumacher
961 SE, Shih J, Kucherlapati MH, Kucherlapati RS, Baylin S, Cope L, Danilova L,
962 Bootwalla MS, Lai PH, Maglinte DT, Berg DJVD, Weisenberger DJ, Auman JT, Balu
963 S, Bodenheimer T, Fan C, Hoadley KA, Hoyle AP, Jefferys SR, Jones CD, Meng S,
964 Mieczkowski PA, Mose LE, Perou AH, Perou CM, Roach J, Shi Y, Simons JV, Skelly
965 T, Soloway MG, Tan D, Veluvolu U, Fan H, Hinoue T, Laird PW, Shen H, Zhou W,
966 Bellair M, Chang K, Covington K, Creighton CJ, Dinh H, Doddapaneni H, Donehower
967 LA, Drummond J, Gibbs RA, Glenn R, Hale W, Han Y, Hu J, Korchina V, Lee S,
968 Lewis L, Li W, Liu X, Morgan M, Morton D, Muzny D, Santibanez J, Sheth M,
969 Shinbrot E, Wang L, Wang M, Wheeler DA, Xi L, Zhao F, Hess J, Appelbaum EL,
970 Bailey M, Cordes MG, Ding L, Fronick CC, Fulton LA, Fulton RS, Kandoth C, Mardis
971 ER, McLellan MD, Miller CA, Schmidt HK, Wilson RK, Crain D, Curley E, Gardner J,
972 Lau K, Mallery D, Morris S, Paulauskis J, Penny R, Shelton C, Shelton T, Sherman
973 M, Thompson E, Yena P, Bowen J, Gastier-Foster JM, Gerken M, Leraas KM,
974 Lichtenberg TM, Ramirez NC, Wise L, Zmuda E, Corcoran N, Costello T, Hovens C,
975 Carvalho AL, Carvalho AC de, Fregnani JH, Longatto-Filho A, Reis RM,
976 Scapulatempo-Neto C, Silveira HCS, Vidal DO, Burnette A, Eschbacher J, Hermes
977 B, Noss A, Singh R, Anderson ML, Castro PD, Ittmann M, Huntsman D, Kohl B, Le
978 X, Thorp R, Andry C, Duffy ER, Lyadov V, Paklina O, Setdikova G, Shabunin A,
979 Tavobilov M, McPherson C, Warnick R, Berkowitz R, Cramer D, Feltmate C,
980 Horowitz N, Kibel A, Muto M, Raut CP, Malykh A, Barnholtz-Sloan JS, Barrett W,
981 Devine K, Fulop J, Ostrom QT, Shimmel K, Wolinsky Y, Sloan AE, Rose AD,
982 Giuliante F, Goodman M, Karlan BY, Hagedorn CH, Eckman J, Harr J, Myers J,
983 Tucker K, Zach LA, Deyarmin B, Hu H, Kvecher L, Larson C, Mural RJ, Somiari S,
984 Vicha A, Zelinka T, Bennett J, Iacocca M, Rabeno B, Swanson P, Latour M,
985 Lacombe L, Têtu B, Bergeron A, McGraw M, Staugaitis SM, Chabot J, Hibshoosh H,
986 Sepulveda A, Su T, Wang T, Potapova O, Voronina O, Desjardins L, Mariani O,
987 Roman-Roman S, Sastre X, Stern M-H, Cheng F, Signoretti S, Berchuck A, Bigner
988 D, Lipp E, Marks J, McCall S, McLendon R, Secord A, Sharp A, Behera M, Brat DJ,
989 Chen A, Delman K, Force S, Khuri F, Magliocca K, Maithel S, Olson JJ, Owonikoko
990 T, Pickens A, Ramalingam S, Shin DM, Sica G, Meir EGV, Zhang Hongzheng,
991 Eijckenboom W, Gillis A, Korpershoek E, Looijenga L, Oosterhuis W, Stoop H,
992 Kessel KE van, Zwarthoff EC, Calatozzolo C, Cuppini L, Cuzzubbo S, DiMeco F,
993 Finocchiaro G, Mattei L, Perin A, Pollo B, Chen C, Houck J, Lohavanichbutr P,
994 Hartmann A, Stoehr C, Stoehr R, Taubert H, Wach S, Wullich B, Kycler W, Murawa

995 D, Wiznerowicz M, Chung K, Edenfield WJ, Martin J, Baudin E, Bubley G, Bueno R,
996 Rienzo AD, Richards WG, Kalkanis S, Mikkelsen T, Noushmehr H, Scarpace L,
997 Girard N, Aymerich M, Campo E, Giné E, Guillermo AL, Bang NV, Hanh PT, Phu BD,
998 Tang Y, Colman H, Evason K, Dottino PR, Martignetti JA, Gabra H, Juhl H,
999 Akeredolu T, Stepa S, Hoon D, Ahn K, Kang KJ, Beuschlein F, Breggia A, Birrer M,
1000 Bell D, Borad M, Bryce AH, Castle E, Chandan V, Cheville J, Copland JA, Farnell M,
1001 Flotte T, Giama N, Ho T, Kendrick M, Kocher J-P, Kopp K, Moser C, Nagorney D,
1002 O'Brien D, O'Neill BP, Patel T, Petersen G, Que F, Rivera M, Roberts L, Smallridge
1003 R, Smyrk T, Stanton M, Thompson RH, Torbenson M, Yang JD, Zhang L, Brimo F,
1004 Ajani JA, Gonzalez AMA, Behrens C, Bondaruk J, Broaddus R, Czerniak B, Esmaeli
1005 B, Fujimoto J, Gershenwald J, Guo C, Lazar AJ, Logothetis C, Meric-Bernstam F,
1006 Moran C, Ramondetta L, Rice D, Sood A, Tamboli P, Thompson T, Troncoso P,
1007 Tsao A, Wistuba I, Carter C, Haydu L, Hersey P, Jakrot V, Kakavand H, Kefford R,
1008 Lee K, Long G, Mann G, Quinn M, Saw R, Scolyer R, Shannon K, Spillane A, Stretch
1009 J, Synott M, Thompson J, Wilmott J, Al-Ahmadie H, Chan TA, Ghossein R, Gopalan
1010 A, Levine DA, Reuter V, Singer S, Singh B, Tien NV, Broudy T, Mirsaidi C, Nair P,
1011 Drwiega P, Miller J, Smith J, Zaren H, Park J-W, Hung NP, Kebebew E, Linehan
1012 WM, Metwalli AR, Pacak K, Pinto PA, Schiffman M, Schmidt LS, Vocke CD,
1013 Wentzensen N, Worrell R, Yang H, Moncrieff M, Goparaju C, Melamed J, Pass H,
1014 Botnariuc N, Caraman I, Cernat M, Chemencedji I, Clipca A, Doruc S, Gorincioi G,
1015 Mura S, Pirtac M, Stancul I, Tcaciuc D, Albert M, Alexopoulou I, Arnaout A, Bartlett J,
1016 Engel J, Gilbert S, Parfitt J, Sekhon H, Thomas G, Rassl DM, Rintoul RC, Bifulco C,
1017 Tamakawa R, Urba W, Hayward N, Timmers H, Antenucci A, Facciolo F, Grazi G,
1018 Marino M, Merola R, Krijger R de, Gimenez-Roqueplo A-P, Piché A, Chevalier S,
1019 McKercher G, Birsoy K, Barnett G, Brewer C, Farver C, Naska T, Pennell NA,
1020 Raymond D, Schilero C, Smolenski K, Williams F, Morrison C, Borgia JA, Liptay MJ,
1021 Pool M, Seder CW, Junker K, Omberg L, Dinkin M, Manikhas G, Alvaro D, Bragazzi
1022 MC, Cardinale V, Carpino G, Gaudio E, Chesla D, Cottingham S, Dubina M,
1023 Moiseenko F, Dhanasekaran R, Becker K-F, Janssen K-P, Slotta-Huspenina J,
1024 Abdel-Rahman MH, Aziz D, Bell S, Cebulla CM, Davis A, Duell R, Elder JB, Hilty J,
1025 Kumar B, Lang J, Lehman NL, Mandt R, Nguyen P, Pilarski R, Rai K, Schoenfield L,
1026 Senecal K, Wakely P, Hansen P, Lechan R, Powers J, Tischler A, Grizzle WE,
1027 Sexton KC, Kastl A, Henderson J, Porten S, Waldmann J, Fassnacht M, Asa SL,
1028 Schadendorf D, Couce M, Graefen M, Huland H, Sauter G, Schlomm T, Simon R,
1029 Tennstedt P, Olabode O, Nelson M, Bathe O, Carroll PR, Chan JM, Disaia P, Glenn
1030 P, Kelley RK, Landen CN, Phillips J, Prados M, Simko J, Smith-McCune K,
1031 VandenBerg S, Roggin K, Fehrenbach A, Kendler A, Sifri S, Steele R, Jimeno A,
1032 Carey F, Forgie I, Mannelli M, Carney M, Hernandez B, Campos B, Herold-Mende C,
1033 Jungk C, Unterberg A, Deimling A von, Bossler A, Galbraith J, Jacobus L, Knudson
1034 M, Knutson T, Ma D, Milhem M, Sigmund R, Godwin AK, Madan R, Rosenthal HG,
1035 Adebamowo C, Adebamowo SN, Boussioutas A, Beer D, Giordano T, Mes-Masson
1036 A-M, Saad F, Bocklage T, Landrum L, Mannel R, Moore K, Moxley K, Postier R,
1037 Walker J, Zuna R, Feldman M, Valdivieso F, Dhir R, Luketich J, Pinero EMM,
1038 Quintero-Aguilo M, Carlotti CG, Santos JSD, Kemp R, Sankarankuty A, Tirapelli D,
1039 Catto J, Agnew K, Swisher E, Creaney J, Robinson B, Shelley CS, Godwin EM,
1040 Kendall S, Shipman C, Bradford C, Carey T, Haddad A, Moyer J, Peterson L, Prince
1041 M, Rozek L, Wolf G, Bowman R, Fong KM, Yang I, Korst R, Rathmell WK,
1042 Fantacone-Campbell JL, Hooke JA, Kovatich AJ, Shriver CD, DiPersio J, Drake B,
1043 Govindan R, Heath S, Ley T, Tine BV, Westervelt P, Rubin MA, Lee JI, Aredes ND,
1044 Mariamidze A, Cherniack AD, Beroukhim R, Meyerson M. 2018. Genomic and
1045 Functional Approaches to Understanding Cancer Aneuploidy. *Cancer Cell* 33:676-
1046 689.e3. doi:10.1016/j.ccell.2018.03.007
1047 Thomas A, Routh ED, Pullikuth A, Jin G, Su J, Chou JW, Hoadley KA, Print C, Knowlton N,
1048 Black MA, Demaria S, Wang E, Bedognetti D, Jones WD, Mehta GA, Gatza ML,
1049 Perou CM, Page DB, Triozzi P, Miller LD. 2018. Tumor mutational burden is a

1050 determinant of immune-mediated survival in breast cancer. *Oncoimmunology* 7.
1051 doi:10.1080/2162402X.2018.1490854
1052 Thorsson V, Gibbs DL, Brown SD, Wolf D, Bortone DS, Ou Yang T-H, Porta-Pardo E, Gao
1053 GF, Plaisier CL, Eddy JA, Ziv E, Culhane AC, Paull EO, Sivakumar IKA, Gentles AJ,
1054 Malhotra R, Farshidfar F, Colaprico A, Parker JS, Mose LE, Vo NS, Liu J, Liu Y,
1055 Rader J, Dhankani V, Reynolds SM, Bowlby R, Califano A, Cherniack AD,
1056 Anastassiou D, Bedognetti D, Rao A, Chen K, Krasnitz A, Hu H, Malta TM,
1057 Noushmehr H, Pedamallu CS, Bullman S, Ojesina AI, Lamb A, Zhou W, Shen H,
1058 Choueiri TK, Weinstein JN, Guinney J, Saltz J, Holt RA, Rabkin CE, Cancer Genome
1059 Atlas Research Network, Lazar AJ, Serody JS, Demicco EG, Disis ML, Vincent BG,
1060 Shmulevich L. 2018. The Immune Landscape of Cancer. *Immunity* 48:812-830.e14.
1061 doi:10.1016/j.immuni.2018.03.023
1062 Turan T, Kannan D, Patel M, Matthew Barnes J, Tanlimco SG, Lu R, Halliwill K, Kongpachith
1063 S, Kline DE, Hendrickx W, Cesano A, Butterfield LH, Kaufman HL, Hudson TJ,
1064 Bedognetti D, Marincola F, Samayoa J. 2018. Immune oncology, immune
1065 responsiveness and the theory of everything. *J Immunother Cancer* 6:50.
1066 doi:10.1186/s40425-018-0355-5
1067 Van Allen EM, Miao D, Schilling B, Shukla SA, Blank C, Zimmer L, Sucker A, Hillen U,
1068 Foppen MHG, Goldinger SM, Utikal J, Hassel JC, Weide B, Kaehler KC, Loquai C,
1069 Mohr P, Gutzmer R, Dummer R, Gabriel S, Wu CJ, Schadendorf D, Garraway LA.
1070 2015. Genomic correlates of response to CTLA-4 blockade in metastatic melanoma.
1071 *Science* 350:207–211. doi:10.1126/science.aad0095
1072 Varn FS, Wang Y, Mullins DW, Fiering S, Cheng C. 2017. Systematic pan-cancer analysis
1073 reveals immune cell interactions in the tumor microenvironment. *Cancer Res*
1074 77:1271–1282. doi:10.1158/0008-5472.CAN-16-2490
1075 Wang B, Liu G, Ding L, Zhao J, Lu Y. 2018. FOXA2 promotes the proliferation, migration
1076 and invasion, and epithelial mesenchymal transition in colon cancer. *Exp Ther Med*
1077 16:133–140. doi:10.3892/etm.2018.6157
1078 Wang E, Bedognetti D, Marincola FM. 2013a. Prediction of Response to Anticancer
1079 Immunotherapy Using Gene Signatures. *J Clin Oncol* 31:2369–2371.
1080 doi:10.1200/JCO.2013.49.2157
1081 Wang E, Bedognetti D, Tomei S, Marincola FM. 2013b. Common pathways to tumor
1082 rejection. *Ann N Y Acad Sci* 1284:75–79. doi:10.1111/nyas.12063
1083 Wang E, Worschech A, Marincola FM. 2008. The immunologic constant of rejection. *Trends*
1084 *Immunol* 29:256–262. doi:10.1016/j.it.2008.03.002
1085 Zou H, Hastie T. 2005. Regularization and Variable Selection via the Elastic Net. *J R Stat*
1086 *Soc Ser B Stat Methodol* 67:301–320.
1087
1088

Author contributions

J.R. contributed to the conception and design of the work, data acquisition and data interpretation, performed data analysis, and drafted the manuscript;

W.H. contributed to the conception and design of the work, data acquisition and data interpretation, performed data analysis, and drafted the manuscript;

P.K. contributed to the design of the work, interpretation of data, and substantively revised the manuscript;

R.M. contributed to analysis and interpretation of data;

G.Z. contributed to the analysis and substantively revised the manuscript;

M.S. contributed to interpretation of data and revision of manuscript;

K.H. contributed to the analysis and revision of manuscript;

G.C. contributed to interpretation of data;

D.R. contributed to the acquisition and analysis, interpretation of data, and revision of manuscript;

J.D. contributed to data interpretation and writing of the manuscript;

L.D. contributed to data interpretation and writing of the manuscript;

T.T. contributed to the analysis and revision of manuscript;

J.S. contributed to the analysis and revision of manuscript;

L.C. contributed to data interpretation and writing of the manuscript;

E.W. contributed to data interpretation, and substantively revised the manuscript;

P.F. substantively contributed to the manuscript;

F.B. contributed to data interpretation and writing of the manuscript;

L.M. contributed to the conception and design of the work, interpretation of data, and substantively revised the manuscript;

J.G. contributed to data interpretation and revision of manuscript;

F.M. contributed to data interpretation, and substantively revised the manuscript;

M.C. contributed to the conception and design of the work, data acquisition, data analysis and data interpretation, and substantively revised the manuscript;

D.B. conceived and designed the study, contributed to the acquisition, data analysis and data interpretation, supervised the analysis and drafted the manuscript.

Competing interests

The authors do not have any competing interests to disclose.

AbbVie disclosures:

Tolga Turan, Josue Samayoa, and Michele Ceccarelli are all employees of AbbVie.

Materials and Correspondence

Michele Ceccerelli: mceccarelli@abbvie.com
Wouter Hendrickx: whendrickx@sidra.org
Davide Bedognetti: dbedognetti@sidra.org

Ethics approval and consent to participate

Not applicable.

Availability of data and material

Scripts for analysis are shared on https://github.com/Sidra-TBI-FCO/ISPC.git. Data generated or analyzed during this study are included in this article. Data sheets for results of individual cancer types are available as cancer data sheets at figshare (https://figshare.com/articles/Cancer_Datasheets/7937246).

Funding

This research has been supported by Qatar Foundation, Qatar National Research Fund (grant numbers: JSREP07-010-3-005 and NPRP-10-0126-170262 awarded to WH and DB, respectively).

1146 **Figure Legends**

1147

1148 **Figure 1: Immunologic classification of 31 cancer types based on expression of ICR**
1149 **gene signature A.** Consensus cluster matrix of SKCM samples based on RNA-seq
1150 expression values of ICR genes (left panel). RNA-seq expression heatmap of ICR genes
1151 annotated with ICR consensus clusters (n = 469). Clusters with intermediate ICR gene
1152 expression levels (ICR Medium1 and ICR Medium2) were combined to obtain ICR High,
1153 Medium and Low groups (HML classification). ICR genes reflect 4 components of immune
1154 mediated tissue rejection: Th1 signaling, CXCR3/CCR5 chemokines, immune effectors and
1155 immune regulatory functions (right panel). **B.** Boxplot of ICR scores across ICR clusters in
1156 31 cancer types. Cancer types are ordered by mean ICR score per cancer. **C.** Forest plot
1157 showing HRs (overall survival) of ICR Low versus High, p-value and number of patients (N)
1158 for each of the cancer types. ICR-enabled cancer types (HR > 1; $p < 0.1$) are indicated with
1159 orange asterisks and ICR-disabled cancer types (HR < 1; $p > 0.1$) are indicated with purple
1160 asterisks. Cancer types PCPG, THYM and TGCT are excluded from the plot, because
1161 confidence intervals ranged from 0 to infinite due to low number of deaths in these cancer
1162 types. **D.** Kaplan Meier curves showing OS across two three different ICR groups in ICR-
1163 enabled and ICR-disabled cancer types.
1164 (Figures of panel A and Kaplan Meier curves for each individual cancer type are available in
1165 the cancer datasheets).

1166

1167 **Figure 2: Deconvolution of immune cell populations and enrichment of oncogenic**
1168 **pathways through single sample GSEA**. **A.** Heatmap of enrichment values for cell-specific
1169 immune-signatures as described by Bindea *et al*. Samples are ordered by ICR cluster and
1170 ordered by cancer type within ICR clusters. **B.** Pearson coefficient of correlation between
1171 ICR score and enrichment scores of oncogenic pathways per cancer. Pathways that have a
1172 positive correlation with ICR are green and those with an inverse correlation are blue.

1173

1174 **Figure 3: Association of ICR with nonsilent mutation rate, predicted neoantigen load,**
1175 **and tumor aneuploidy. A.** Scatter plot of log transformed nonsilent mutation count per ICR
1176 cluster for each cancer type. **B.** Log transformed predicated neoantigen load per ICR cluster
1177 for each cancer type. **A.B.** Red crossbar represents the mean value per ICR cluster. Cancer
1178 types are ordered by mean nonsilent mutation count per cancer. Nonsilent mutation rate and
1179 predicted neoantigen load were obtained from Thorsson et al (Thorsson et al., 2018). **C.**
1180 Correlation between aneuploidy score and raw/purity adjusted ICR score for all cohorts with
1181 significant relationships between ICR and aneuploidy.

1182

Figure 4: Relationship between ICR score and mutations in individual genes. A. Top 35 of mutated genes with negative non-zero coefficients of a trained elastic net model identified genes whose mutation is associated with a decrease of the ICR (left panel). Top 35 mutated genes with a positive association with ICR score in pan-cancer trained model (right panel). Contributions of each individual cancer type to the coefficient in trained elastic net model are proportionally indicated by size of the bars. **B.** Ratio of mean ICR score in mutated samples and ICR score in WT samples. Cancer types are ordered manually based on patterns of calculated ratios.

Figure 5: Pan-cancer clustering based on oncogenic pathway enrichment segregates ICR-enabled and ICR-disabled cancer types. A. Heatmap of enrichment scores of selected oncogenic pathways, samples are hierarchically clustered in two main clusters: one cluster consists mostly of ICR-enabled cancer types (ICR beneficial cluster), while the second cluster contains all samples from ICR-disabled cancer types (ICR non-beneficial cluster). **B.** Kaplan-Meier OS curves for ICR High, Medium, and Low clusters for samples in the ICR beneficial and ICR non-beneficial cluster separately. **C.** Subgroup survival analysis of all samples of ICR-neutral cancer types clustered in the ICR beneficial cluster and ICR non-beneficial cluster.

Figure 6: Examples of pan-cancer binary classifications based on enrichment of individual tumor intrinsic gene signatures and corresponding stratified pan-cancer survival analysis. A. Histogram showing pan-cancer classification based on median pan-cancer enrichment value of the proliferation signature as described by Miller *et al*(Miller et al., 2016) (Proliferation Low: ES is lower than median ES observed pan-cancer; Proliferation High: ES is higher or equal to median ES observed pan-cancer). **B.** Pan-cancer Kaplan Meier curves of ICR groups stratified by Proliferation High (left panel) and Proliferation Low (right panel) groups corresponding to classification as shown in panel A. **C.** Histogram showing pan-cancer classification based on pan-cancer enrichment values of the Hallmark pathway TGF-ß signaling. **D.** Pan-cancer Kaplan Meier curves stratified by TGF-ß signaling Low (left panel) and TGF-ß signaling High (right panel) groups corresponding to classification as shown in panel C.

Figure 7: Conditional predictive value of ICR for response to immune checkpoint treatment. A. Predictive value of ICR across public datasets with response to immune checkpoint treatment indicated by p-value of two-sided t-test comparing ICR score in samples

of responding versus non-responding patients. ICR score was highest in response group for all significant comparisons. Response was defined as long-survival or response in the van Allen dataset, stable disease, partial response (PR) and complete response (CR) in the Chen dataset, and as PRCR in Riaz, Hugo and Prat datasets. **B.** Boxplot of ICR score in "nonresponse" compared with "long-survival or response" to anti-CTLA4 treatment in van Allen dataset (left). Boxplots of subgroup analysis of proliferation groups (middle) and TGF-ß signaling groups (right). P-value of t-test comparing means are indicated in the plot. **C.** Kaplan Meier curves showing OS across ICR tertiles in all samples (left), across proliferation (middle), and TGF-ß signaling subgroups (left).

Supplementary Figures

Supplementary Figure 1: Pearson correlation between RNA-seq expression values of ICR genes for each of the 31 cancer types.

Supplementary Figure 2: Scatterplot showing correlation between ICR score and TIS score(Danaher et al., 2018) (**A**), ICR score and leukocyte fraction (**B**), and ICR score and TIL percentage (**C**). Leukocyte fraction and TIL percentage values were obtained from Thorsson *et al* (Thorsson et al., 2018). Each dot represents a single sample.

Supplementary Figure 3: A. Boxplot showing mean ICR score for each cancer type per group of cancer types: ICR-enabled, ICR-neutral and ICR-disabled. A single dot represents a single cancer type. **B.** Boxplot showing delta between mean ICR score in ICR High cluster compared with mean ICR score in ICR Low cluster. A single dot represents a single cancer type.

Supplementary Figure 4: Pan-cancer Kaplan-Meier curves in ICR-disabled (top left panel) and ICR-enabled (top right panel) groups and stratified analysis by AJCC pathologic stage I & II (middle panels) and stage III & IV (bottom panels).

Supplementary Figure 5: Dotted heatmap showing mean ES for each immune cell population per cancer type, mean ES scores were z-scored per row.

Supplementary Figure 6: A. Scatterplot of mean mutation rate versus mean neoantigen load per cancer type. **B.** Ratio of nonsilent mutation rate between ICR High and ICR Low groups versus the ratio of predicted neoantigen load between in ICR High compared to ICR Low groups. **C.** Ratio of nonsilent mutation rate between ICR High and ICR Low groups

versus mean nonsilent mutation rate. **D.** Ratio of predicted neoantigen load between ICR High compared to ICR Low groups versus mean predicated neoantigen load.

Supplementary Figure 7: A. Boxplot of ICR score by MSI status in COAD (left panel) and STAD (right panel). P-values of t-test to compare mean ICR score per MSI group are indicated in the plot. **B.** Boxplot of number of mutated genes with a negative coefficient in ICR trained elastic net model by MSI status in COAD (left panel) and STAD (right panel). P-values of t-test to compare mean number of mutations per MSI group are indicated in the plot.

Supplementary Figure 8: Table to check overlap between tumor intrinsic pathways genes and frequently mutated genes. When a gene (columns) is part of a gene signature (rows), this is indicated by “YES”, if not, it is indicated by “NO”. Genes that have a negative coefficient in trained model are shown in blue, pathways that inversely correlate with ICR (**Figure 2B**) are indicated in blue. Genes that have a positive coefficient in trained model are shown in red, pathways that positively correlate with ICR (**Figure 2B**) are indicated in red.

Supplementary Figure 9: Scatterplots of each of the combinations of: 1) ICR scores, 2) proliferation ES, 3) TGF-ß signaling ES, and 4) mutation rate (n = 4452). Pearson’s correlation coefficient and regression line (red) are indicated in the plots.

Supplementary Figure 10: Pan-cancer Kaplan Meier curves of ICR groups stratified by both Proliferation High (left panels) and Proliferation Low (right panels) groups (corresponding to classification of shown in **Figure 6A**) and by Mutation rate High (top panels) and Mutation rate Low (bottom panels) based on pan-cancer median mutation rate.

Supplementary Figure 11: Multivariate Cox proportional hazards model including ICR classification, proliferation enrichment, TGF-ß signaling enrichment, and tumor mutation rate.

Supplementary Figure 12: Survival analysis of ICR Low versus ICR High in pathway enrichment categories across 40 pathway signatures (rows) for each cancer type (columns). HRs (hazard ratios) for death in high enrichment categories (**A**) are compared with HRs in low enrichment categories (**B**). **C.** Differences in prognostic impact of ICR classification between pathway signature enrichment categories for each cancer type. HR of ICR Low vs. ICR High was calculated per category from binary classification of enrichment of oncogenic pathway signatures (rows) within individual cancer types (columns). The delta between HR

in the highly enriched group and the HR in the group with low enrichment was calculated for each signature/cancer type combination.

Supplementary Tables

Supplementary Table 1: Association of ICR with OS across 31 cancer types with ICR as a categorical variable ICR Low versus ICR High (first and second column; yellow), and ICR as continuous variable (third and fourth column; blue). HR, hazard ratio for death.

Supplementary Table 2: Comparison of mean ES of samples from ICR-disabled cancer types with mean ES of samples from ICR-enabled cancer types for 54 oncogenic pathway gene signatures.

Supplementary Table 3: Pan-cancer survival analysis stratified by binary classification based on enrichment of selected oncogenic pathway signatures. HR, hazard ratio for death.